Beyond understanding the role of far-field climate in the Gulf of Panama coastal dynamics

an analysis of long-term and seasonal variability of wave systems

Authors
Vallarino-Castillo, Ruby; Antolínez, José A.A.; Negro-Valdecantos, Vicente; Portilla-Yandún, Jesús

DOI
10.1007/s00382-025-08007-w

Publication date
2026

Document Version
Final published version

Published in
Climate Dynamics

Citation (APA)
Vallarino-Castillo, R., Antolínez, J. A. A., Negro-Valdecantos, V., & Portilla-Yandún, J. (2026). Beyond understanding the role of far-field climate in the Gulf of Panama coastal dynamics: an analysis of long-term and seasonal variability of wave systems. *Climate Dynamics*, *64*(2), Article 39. https://doi.org/10.1007/s00382-025-08007-w

Climate Dynamics (2026) 64:39
https://doi.org/10.1007/s00382-025-08007-w

Beyond understanding the role of far-field climate in the Gulf of Panama coastal dynamics: an analysis of long-term and seasonal variability of wave systems

Ruby Vallarino-Castillo[1] · José A. A. Antolínez[2] · Vicente Negro-Valdecantos[1] · Jesús Portilla-Yandún[3]

Received: 24 April 2025 / Accepted: 30 November 2025

Abstract

Understanding wave systems (WS) dynamics in semi-enclosed tropical basins is challenging due to interactions between remote wave generation and regional climate variability. In the Gulf of Panama, prior studies mainly relied on single-site offshore analyses, limiting characterization of wave energy distribution and its atmospheric and oceanic drivers. This gap in knowledge is particularly consequential for coastal hazard assessments and for deciphering ocean–atmosphere interactions in regions influenced by both long-period swells and low-level wind jets. To address this limitation, we present a comprehensive multi-decadal analysis of the seasonal and long-term variability of significant wave height (Hs) and peak wave period (Tp), based on WS identified applying spectral statistical techniques using the GLOSWAC-5 atlas. To understand the variability and the modulating effect of the Gulf of Panama semi-enclosed morphology, three representative sites at its entrance were selected. Monthly patterns were analyzed by classifying wave trains according to relative orientation (i.e., following, crossing, and opposing) to determine the predominant direction and multimodal activity. Long-term trends were assessed over 17 to 18-year intervals (i.e. 1969–1987, 1988–2005, 2006–2023) using exploratory analysis and quantile regression, with results reported separately for the dry season (December–April) and the wet season (May–November). The analysis revealed five dominant WS, each associated with specific generation mechanisms and geographic origins: WS1, associated with Southern Ocean swells; WS5, originating from Northern Hemisphere swells; WS2, driven by southeasterly trade winds from the subtropical Pacific; and two regionally forced systems, WS3 and WS4, generated by the Panama and Chocó Low-Level Jets, respectively. WS1 shows increases in Hs of about 5–10 cm during 1969–1987 and 1988–2005, and up to ~15 cm in 2006–2023, with Tp rising by ~0.3–0.6 s over the same intervals. WS2 exhibits small variations, with Hs ranging from −10 to +17 cm and Tp fluctuations within ±0.3 s across the three intervals. WS3 displays the strongest changes, with median Hs increases of 10–30 cm in the first two intervals and extreme values reaching 50–60 cm in 1988–2005 and 2006–2023, together with Tp increments of ~0.3–0.5 s. WS4 remains comparatively stable in all periods, with Hs variations within ±10 cm and Tp changes <0.4 s. WS5 intensifies mainly in 2006–2023, showing Hs increases of 8–15 cm and Tp rises of ~0.2–0.4 s. Monthly mean Hs anomalies (>0.10 m) at the 50th percentile suggest a relationship with El Niño–Southern Oscillation (ENSO), but analyses using the 95th percentile reveal that only WS2, WS3, and WS4 exhibit a stronger association with ENSO phases.

Keywords Multimodal wave patterns · Wave spectra · Wave systems (WS) · Gulf of Panama · Coastal hazards · El Niño–Southern Oscillation (ENSO)

✉ Ruby Vallarino-Castillo
ruby.vallarino@alumnos.upm.es

[1] Environment, Coast and Ocean Research Laboratory, Universidad Politécnica de Madrid, Campus Ciudad Universitaria, Calle del Profesor Aranguren 3, 28040 Madrid, Spain

[2] Department of Hydraulic Engineering, Faculty of Civil Engineering and Geosciences, Delft University of Technology, Delft, The Netherlands

[3] Research Center of Mathematical Modelling (MODEMAT), Escuela Politécnica Nacional, Quito, Ecuador

Published online: 06 January 2026

1 Introduction

Coastal environments have long been integral to human settlements, a process that has been intensified in the present with rapid population growth. Socio-economic development along with natural climate change has exacerbated the phenomenon of coastal squeeze, leading to environmental degradation, increased erosion, and heightened flood risks (Lincke et al. 2022; Neumann et al. 2015; Reguero et al. 2015). These impacts are influenced by factors such as population density in vulnerable zones, the value of social and economic assets, and the ability of the region to implement coastal protection and community-based mitigation strategies (Calil et al. 2017; Luijendijk et al. 2018). Vulnerability is further amplified in areas situated below 10 m above sea level, where sea-level rise, extreme wave events, and land subsidence pose significant risks (Reguero et al. 2015). Lincke et al. (2022) emphasize that the primary drivers of coastal flooding risk are socioeconomic growth and sea-level changes, with coastal protection resources allocated not only in response to rising sea levels but also to economic development. Also, the risk is concentrated in rural areas, where limited protection capacity worsens the situation, as seen across coastal Latin America (Calil et al. 2017; Lincke et al. 2022). Previous research has highlighted the impacts of shoreline changes and extreme wave events, including those caused by swells or hurricanes/tropical cyclones in the region (Silva et al. 2014; Reguero et al. 2015; Vallarino Castillo et al. 2023).

Data derived from global and regional research on coastline change (Luijendijk et al. 2018; Vousdoukas et al. 2020), sea level rise, and the risk of flooding and economic losses (Vitousek et al. 2017; Lincke et al. 2022), which includes long-term water level variations and short-term storm surges (Muis et al. 2016, 2023; Kirezci et al. 2020), offers a framework to guide efforts in the most affected regions. A critical aspect of these coastal risks is wave dynamics, which include both wind-driven waves and long-period swells. These wave systems (WS) interact within multimodal conditions, influencing sediment transport and coastal erosion, with implications for coastal vulnerability (Hoogervorst 2022; Lira-Loarca and Besio 2022). As waves from different origins converge, the resulting patterns can exacerbate coastal impacts, especially when compounded by rising sea levels. Several studies have emphasized the vulnerability of the Central American region, particularly the Pacific coast of Panama. Projections under the high emissions scenario (i.e., RCP8.5) indicate that this area will experience rising sea levels and more frequent, intense storm surges, making it a potential hotspot for coastal impacts in the Central American Pacific (Reguero et al. 2015; Kirezci et al. 2020). In addition to sea level rise, the influence of ENSO events, which cause rapid water level fluctuations, is significant. Across many coastal zones of the Latin American region (IH Cantabria—CEPAL 2015; Vallarino Castillo et al. 2023), long-term sea level rise contributes more than 1.0 mm per year, while short-term variability associated with El Niño Southern Oscillation (ENSO) events can induce transient increases in sea level exceeding 30 cm. Furthermore, the combined effects of land subsidence, as observed in regions such as parts of Chile, and anthropogenic pressures, including the construction of infrastructure along the shoreline, can intensify coastal squeezing processes. These factors collectively exacerbate shoreline retreat and may lead to significant localized increases in relative sea level. Despite insights from global and regional studies, localized research is necessary to account for the specific morphological conditions, coastal dynamics, and climatic patterns of each study area. Such research is crucial for acquiring the detailed data required to inform national-level planning strategies. This is especially critical in regions where multiple WS converge, requiring an individualized analysis of each system based on its origin. Simplified parameterizations, such as significant wave height (Hs), can oversimplify energy transport by reducing the wave spectrum to a single direction and frequency, failing to capture the complexity of multimodal spectra where multiple wave trains with different wavelengths and propagation directions interact and vary over time (i.e., wave aging). Consequently, adopting more detailed parameterizations that accurately capture these interactions is necessary for enhancing the reliability of energy transport models, which are central to coastal and ocean engineering applications (Holthuijsen 2007; Hoogervorst 2022; Hegermiller et al. 2017; Mori et al. 2013). The relevance of such parameterizations is evident in regions with complex wave climates, where multiple systems interact. In this context, Portilla-Yandún et al. (2020) highlight the multimodal nature of wave conditions in the Colombian Pacific, identifying five systems that shape the coastal climate of the region. Their findings provide a valuable reference for understanding dynamics in adjacent areas, including the Pacific coast of Panama. In the Gulf of Panama, such research is particularly relevant due to the intrinsic vulnerability of the region and the complexity of its coastal morphology and bathymetry, which limit the propagation of certain WS in this semi-enclosed basin (Portilla et al. 2015).

Considering local variations induced by phenomena such as ENSO is crucial, as its different phases significantly alter coastal climates along the American Pacific, potentially intensifying erosion. The study by Losada et al. (2013) provides evidence on how ENSO contributes to sea level rise in Latin America, identifying the Panamanian Pacific as one of the most affected regions. During its positive phases,

ENSO can enhance the frequency and intensity of tropical cyclones in the Pacific while also modifying average and extreme wave conditions, influencing energy, direction, wind speed, and the trajectory of local "Low-Level Jets" (Amador et al. 2006; Amador 2008; Vallarino-Castillo et al. 2024; Odériz et al. 2024). It is important to note that climate variations in coastal areas induced by ENSO phases do not follow a linear pattern but fluctuate seasonally, influencing associated risks. Odériz et al. 2024 highlights that during the colder seasons of each hemisphere, ENSO events significantly impact numerous countries, making it the dominant climatic driver of seasonal variability and associated hazards. The combination of ENSO's positive phases and rising sea levels will increase exposure in the Central American Pacific region. As coastal populations grow and considering that extreme ENSO events, such as the one in 1998, have contributed to sea level rise, an increasing number of people and critical socio-economic resources will face greater risk from coastal flooding (Reguero et al. 2015).

This exploratory study establishes a baseline of multimodal wave conditions at the entrance of the Gulf of Panama, emphasizing their interaction with regional morphology and implications for coastal extreme events. It also describes the long-term and seasonal variability of WS from 1969 to 2023 and considers their possible links to the ENSO. The results provide new insights into the influence of large-scale climate phenomena on local wave dynamics and offer a basis for future wave propagation studies in the basin.

The structure of this study is organized as follows. Section 1 provides a description of the regional context of the Gulf of Panama. Section 2 explains the methodology and statistical techniques used to analyze both general and extreme wave conditions, focusing on long-term trends and seasonality. Section 3 presents the results, including the characterization of the main WS, their temporal variability, and the influence of ENSO phases. Finally, Sect. 4 summarizes the main conclusions of this study, highlighting its contributions to advancing the current understanding of wave conditions in the Gulf of Panama and the potential directions for future research.

2 Methodology

2.1 Geographical context and coastal hazards in the Gulf of Panama

The study area is the entrance to the Gulf of Panama (Fig. 1A1), a region characterized by complex morphology that modulates the impact of wave-generating systems in nearby coastal areas (Bundschuh and Alvarado 2012). Therefore, it is essential to understand how these WS interact outside the gulf and then analyze more deeply how the bathymetry and morphological configuration of the Gulf of Panama may alter their behavior. Prior research has identified zones where converging orthogonal profiles create "bathymetric lenses" that focus wave energy (Grimaldo 2014; Speranski and Calliari 2001).

In the coastal section with the highest wave convergence in the Gulf of Panama, previous studies have shown that the shoreline change indicates an average retreat of −1.07 m/year, based on data from 1998 to 2021 (Vallarino Castillo et al. 2022). In addition, information has been gathered about strong wave events that caused damage to vulnerable housing and critical infrastructure, reported on the social network X (formerly Twitter) (Fig. 1A2). These events tend to concentrate in the main convergence zone (Playa Farallón—Playa Punta Chame), coinciding with the most affected coastal region, while isolated occurrences have been reported in other Pacific and Caribbean areas of Panama (see Grimaldo 2014 for further details). The beaches of the Gulf affected by these strong wave events mostly show shoreline retreat categorized as "moderate erosion" (with rates ranging from 0 m/year to −1.0 m/year) or "high erosion" (with rates > −1.0 m/year). However, Playa de Farallon presents an exception: although it is classified as "moderate accretion" (with rates between 0 m/year and 1.0 m/year) on average, in the coastal section where damage to vulnerable houses has been recorded, a localized retreat greater than -2.00 m/year has been observed, increasing its vulnerability compared to other beaches in the region (Fig. 1D). Since these events are recurrent mainly in the months of May, September, and October, during the wet (rainy) season (Fig. 1B and C), it is necessary to conduct both long-term and seasonal analyses to identify relationships between external and local wave-generating systems that may influence the variability of wave patterns throughout the year.

Providing this context is essential (Fig. 1), as it situates the Gulf of Panama within the broader framework of external wave-generating systems and shows how local morphology at the gulf entrance modulates their impact. Given the recurrent flooding and coastal erosion events in the region and the scarcity of long-term local wave data, understanding these interactions is crucial. This serves as a baseline for future studies on wave propagation aimed at understanding the wave climate dynamics throughout the Gulf of Panama, while noting that the present analysis focuses exclusively on conditions outside the gulf.

2.2 Wave data analysis and statistical approach

A preliminary analysis of wave conditions outside the Gulf of Panama will be conducted to identify the main WS that

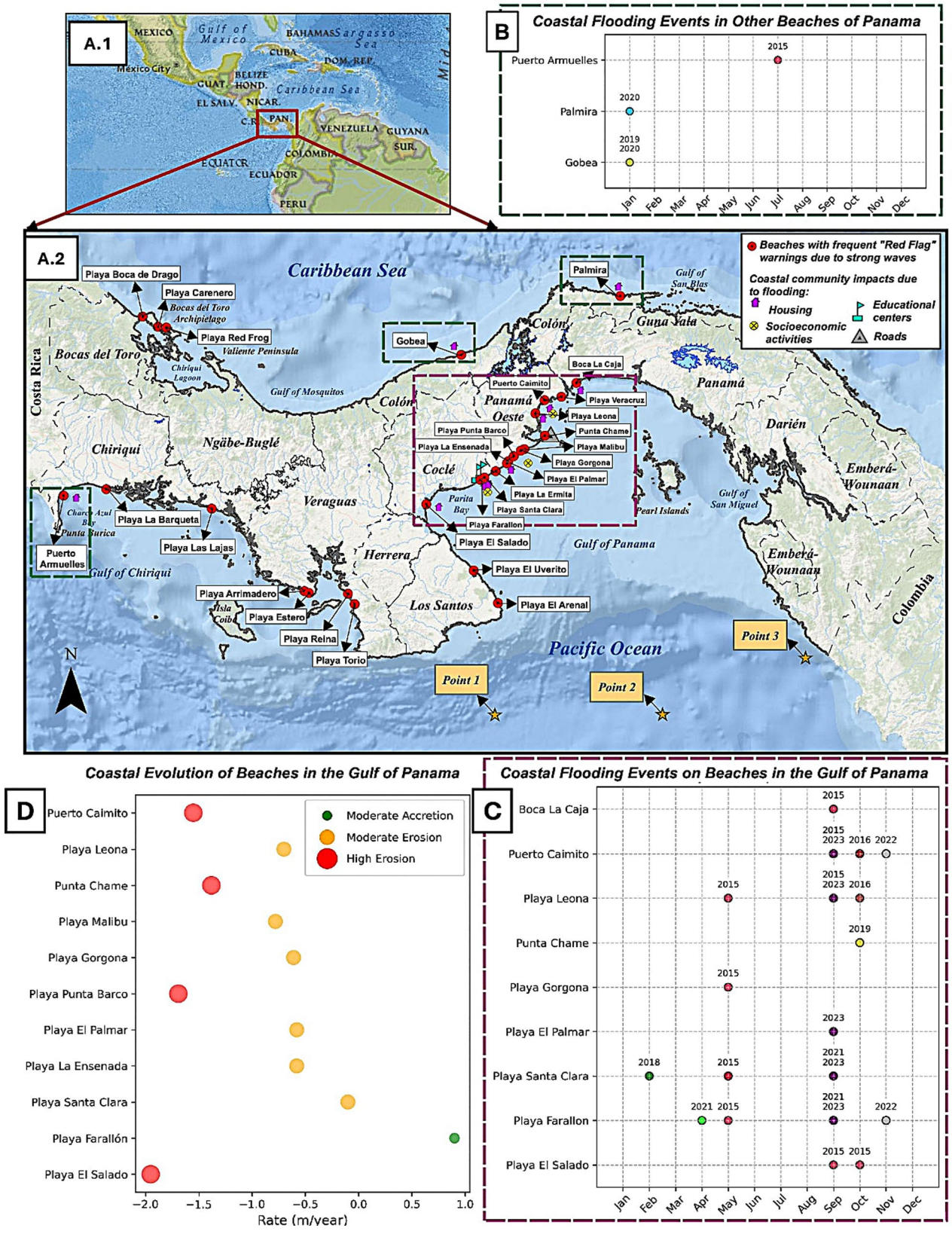
A.1
MEXICO
Gulf of Mexico
BAHAMAS
Sargasso Sea
CUBA
DOM. REP.
México City
BELIZE
GUAT.
HOND.
Caribbean Sea
EL SALV.
NICAR.
C.R.
PAN.
VENEZUELA
GUYANA
SUR.
COLOMBIA
ECUATOR
ECUADOR
PERU
B
Coastal Flooding Events in Other Beaches of Panama
Puerto Armuelles
Palmira
Gobea
2015
2020
2019
2020
Jan Feb Mar Apr May Jun Jul Aug Sep Oct Nov Dec
A.2
Caribbean Sea
Beaches with frequent "Red Flag" warnings due to strong waves
Coastal community impacts due to flooding:
Housing
Socioeconomic activities
Educational centers
Roads
Playa Boca de Drago
Playa Carenero
Bocas del Toro Archipielago
Playa Red Frog
Valiente Peninsula
Bocas del Toro
Chiriqui Lagoon
Gulf of Mosquitos
Costa Rica
Chiriqui
Ngäbe-Buglé
Veraguas
Herrera
Los Santos
Coclé
Colón
Panamá Oeste
Panamá
Darién
Guna Yala
Emberá-Wounaan
Gulf of San Blas
Gulf of San Miguel
Pearl Islands
Gulf of Panama
Gulf of Chiriqui
Pacific Ocean
Colombia
Palmira
Gobea
Boca La Caja
Puerto Caimito
Playa Veracruz
Playa Leona
Playa Punta Barco
Punta Chame
Playa La Ensenada
Playa Malibu
Playa Gorgona
Playa El Palmar
Playa La Ermita
Parita Bay
Playa Santa Clara
Playa Farallon
Playa El Salado
Playa El Uverito
Playa El Arenal
Playa La Barqueta
Playa Las Lajas
Puerto Armuelles
Playa Arrimadero
Isla Coiba
Playa Estero
Playa Reina
Playa Torio
Point 1
Point 2
Point 3
N
D
Coastal Evolution of Beaches in the Gulf of Panama
Moderate Accretion
Moderate Erosion
High Erosion
Puerto Caimito
Playa Leona
Punta Chame
Playa Malibu
Playa Gorgona
Playa Punta Barco
Playa El Palmar
Playa La Ensenada
Playa Santa Clara
Playa Farallón
Playa El Salado
−2.0 −1.5 −1.0 −0.5 0.0 0.5 1.0
Rate (m/year)
C
Coastal Flooding Events on Beaches in the Gulf of Panama
Boca La Caja
Puerto Caimito
Playa Leona
Punta Chame
Playa Gorgona
Playa El Palmar
Playa Santa Clara
Playa Farallon
Playa El Salado
2015
2015 2023 2016 2022
2015 2023 2016
2015
2019
2015
2023
2018 2015
2021 2023
2021 2015 2021 2023 2022
2015 2015
Jan Feb Mar Apr May Jun Jul Aug Sep Oct Nov Dec

Fig. 1 **A1** Regional map showing the location of the study area. **A2** Local map (zoomed in) highlighting beaches frequently affected by strong wave advisories and sites reporting damage to vulnerable housing, critical infrastructure, and economic activities. **B** Timeline of coastal flooding events reported for other beaches along the coasts of Panama (Caribbean Sea and Gulf of Chiriquí), included for regional context. **C** Timeline of coastal flooding events documented in the Gulf of Panama, corresponding to the study area. **D** Approximate classification of erosion and accretion rates for beaches in the Gulf of Panama. Note: Flooding dates (**B**–**C**) and shoreline-change estimates (**D**) were compiled by the authors

shape the multimodal sea state in this area, the data from the GLOSWAC-5 atlas (GLObal Spectral Wave Climate, see https://gloswac.epn.edu.ec/) will be used. This atlas provide s a database on the spectral characterization of ocean waves. It is based on ERA-5 reanalysis data provided by ECMWF, covering a 54-year period, from 1969 to 2023. GLOSWAC-5 is an update of the original GLOSWAC, which previously relied on ERA-Interim reanalysis data for a 37-year period (1979–2015) (Portilla-Yandún 2018; Portilla-Yandún and Bidlot 2025). The GLOSWAC-5 atlas offers long-term density distributions of frequency (f) and direction (θ) of the spectrum, segmented into wave partitions and systems at different ocean locations, according to the geographical sites of the reanalysis data. Since the wavefield may consist of multiple wave trains with different propagation directions and periods, the spectrum is partitioned based on the so called watershed algorithm (Hasselmann et al. 1996). Each partition includes a set of frequency-directional bins that describe a specific group of waves. These partitions are grouped into different clusters called "wave systems (WS)" or "wave families," which share similarities in frequency and direction. These systems may be related to atmospheric origins, both external and local (Portilla-Yandún et al. 2015; Portilla-Yandún 2018).

At the entrance to the Gulf of Panama, the GLOSWAC-5 atlas provides information for 10 distinct WS across three nearby geographic locations: Site 1 (Point 1) at 6.84°N, 80.04°W; Site 2 (Point 2) at 6.84° N, 78.95° W; and Site 3 (Point 3) at 7.20° N, 78.02° W (see Fig. 2).

This study first employs an analysis of the monthly occurrence frequency and Hs average, for each wave system, providing a descriptive framework for the annual behavior of these systems. This stage aims to identify seasonal patterns, establishing a quantitative basis for understanding the complexity of the wave spectrum at the entrance of the Gulf of Panama. Simultaneously, wave trains corresponding to the period 1969–2023 are analyzed and classified into three categories based on their relative angle to the primary wave train: following waves (0°–45°), crossing waves (45°–135°), and opposing waves (>135°). The classification of these categories follows methodologies established in the literature (Donelan et al. 1997; Davison et al. 2022), allowing for the determination of the predominant wave direction and the frequency of each type at three geographical sites within the study area. In this context, correlation analysis between different WS at each location supports the information presented in the previous section regarding their genesis, whether driven by large-scale climatic phenomena of global origin or regional mechanisms such as the Central America Wind Jets. Additionally, based on the results, the potential impact of the semi-enclosed morphology of the Gulf of Panama on wave dynamics is described.

To detect long-term trends in Hs variability, data were grouped into intervals series of approximately 17 to 18 years periods (1969–1987, 1988–2005, and 2006–2023). Each group also incorporated the seasonal component by segregating interannual data for the dry and wet seasons. This data structuring facilitates comparisons through exploratory statistical analyses, including the description of Hs distributions using histograms, evaluation of data dispersion using the Levene test, which assesses the homogeneity of variances among groups (Levene 1960), and the comparison of the central distribution of WS using the Mann–Whitney U test (Gastwirth et al. 2009; McKnight and Najab 2010). The initial approach, centered on the complete distribution of Hs data, serves as the basis for interpreting the overall behavior of WS across different time periods. Following this comprehensive analysis, the study proceeds with a preliminary assessment of outliers, defined as values exceeding the upper threshold ($q3+1.5\cdot(q3-q1)$), where q1 and q3 correspond to the first and third quartiles (25th and 75th percentiles) of the distribution within each period. This approach highlights changes in the distribution tail that may have direct implications for coastal responses, including shoreline changes and the potential impacts of high-magnitude wave events on vulnerable coastal areas (see Fig. 1, panel A.2).

Building on this, a quantile regression analysis is conducted for each period, maintaining data segmentation according to the dry and wet seasons. The selection of the 50th, 95th, and 99th quantiles allow for a deep trend analysis of both the central value and the extremes of the Hs distribution. While the 50th quantile reflects the median behavior, the 95th and 99th quantiles provide key insights into the variability of high-magnitude events, each with a distinct and complementary approach. The 95th quantile captures changes in high but relatively frequent values within the distribution, which may indicate a progressive intensification of wave conditions. Conversely, the 99th quantile focuses on the most extreme events, such as intense storms or exceptional wave pulses, which can exacerbate existing erosion problems in the beaches of the Gulf of Panama. Analyzing these two quantiles separately makes it possible to differentiate between a general intensification of wave conditions and specific increases in anomalous

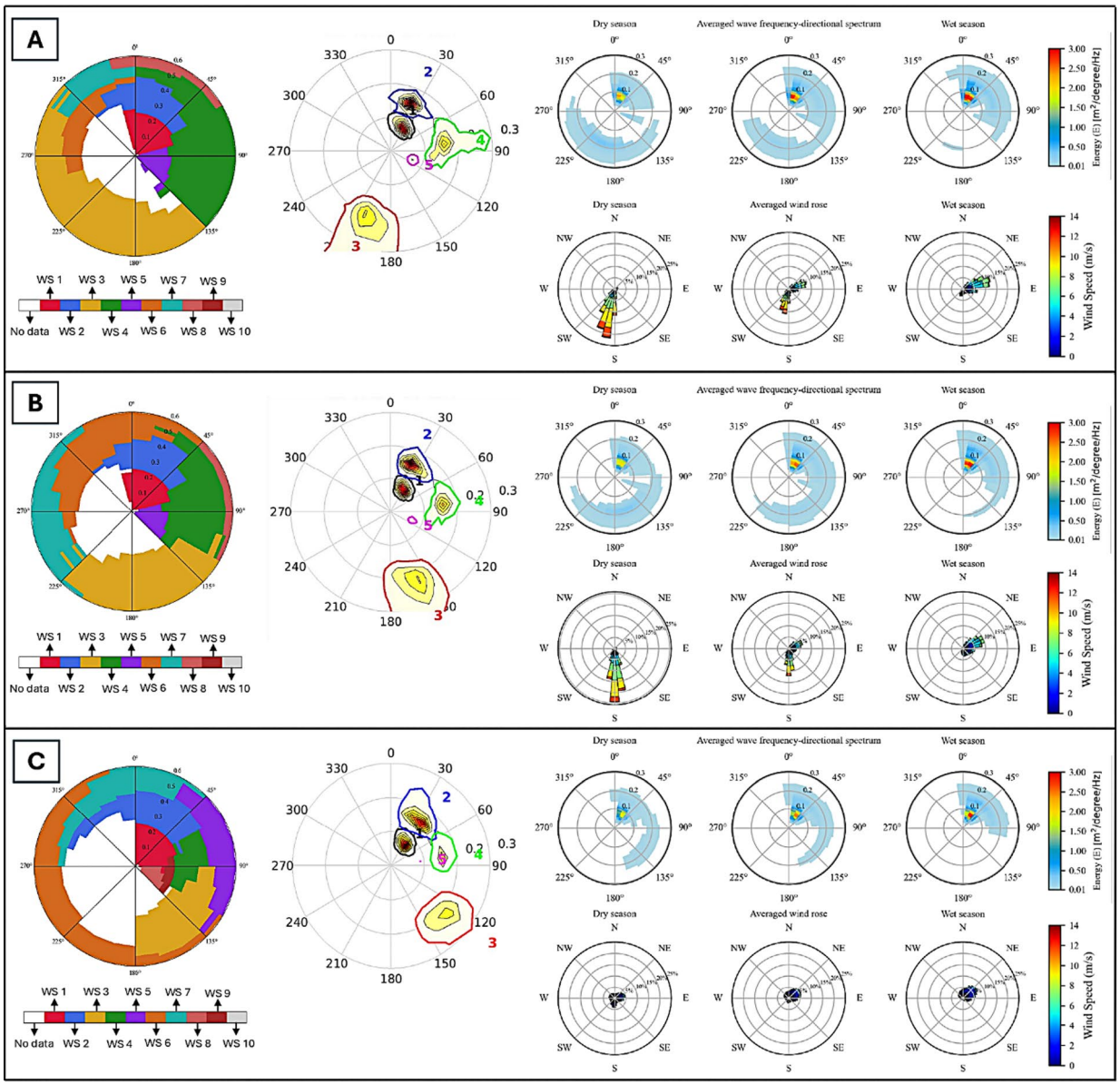
A
B
C
WS 1
WS 3
WS 5
WS 7
WS 9
No data
WS 2
WS 4
WS 6
WS 8
WS 10
Dry season
Averaged wave frequency-directional spectrum
Wet season
Averaged wind rose
Energy (E) [m²/degree/Hz]
Wind Speed (m/s)

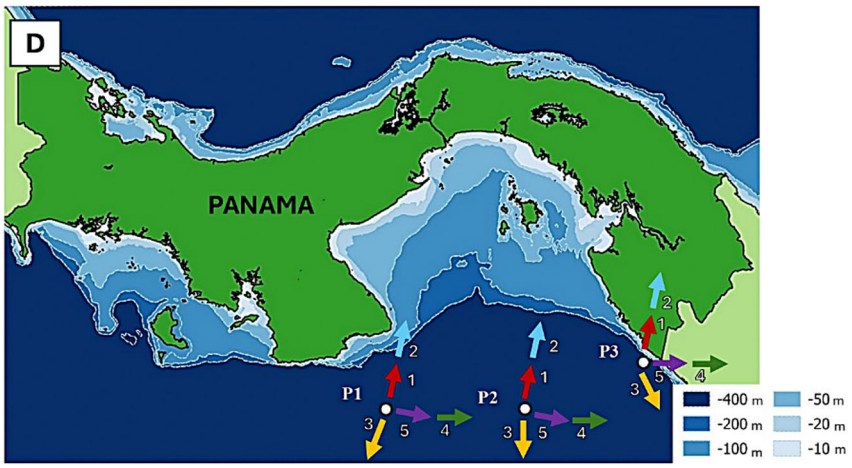
D
PANAMA
P1
P2
P3
-400 m
-200 m
-100 m
-50 m
-20 m
-10 m

Fig. 2 The total set of WS and the dominant systems identified at the entrance to the Gulf of Panama are shown. The average and seasonal frequency-direction energy spectra, along with wind roses for the entire period (1969–2023), are shown for: **A** Site 1/Point 1, **B** Site 2/Point 2, and **C** Site 3/Point 3. **D** Map indicating the location of the three offshore study sites at the entrance of the Gulf of Panama. The arrows represent the direction toward which the main WS propagate (arrows may extend over land areas due to their size but only indicate propagation direction)

events. Quantile regression is particularly robust for detecting trends in these extreme quantiles compared to simple linear regression, which primarily fits central values and may not adequately capture variations in the most intense events (Hao and Naiman 2007).

As a complementary analysis, given the significant role of the peak wave period (Tp) in combination with Hs, the monthly variability of Tp is analyzed within each time interval.. This analysis extends to the identification of the co-occurrence of Tp and the Hs outliers, aiming to identify possible associations between simultaneous increases in both variables. Such patterns could indicate an increase in the presence of swell-generated waves or distant storm waves, which are characterized by greater energy and wider spacing, conditions that contribute to long-term coastal erosion.

Finally, considering the geographical position of the study area, within the Eastern Tropical Pacific, a region historically influenced by ENSO phenomena, correlation analyses were conducted between ENSO indices and the data exceeding the 50th percentile. A sliding window approach with intervals of 5 and 10 months was used to effectively capture the immediate variability associated with ENSO events. The analyses employed monthly anomaly data provided by NOAA Physical Sciences Laboratory (PSL), using indices commonly applied in large-scale studies, such as Niño 3.4 and Niño 3, as well as Niño 1+2, which captures more continental-scale impacts, particularly along the coasts of Peru and Ecuador. Correlating periods of heightened ENSO activity with observed changes in WS further helps identify their contribution to the regional wave climate.

3 Results

3.1 Seasonal variability and characteristics of wave systems at the Gulf entrance

At the entrance of the Gulf of Panama, five primary WS (i.e., WS1–WS5) have been identified (Table 1), consistent with large-scale atmospheric drivers documented in prior studies (Portilla et al. 2015; Portilla-Yandún, 2018; IH-Cantabria 2021; Odériz et al. 2021; Mazzaretto and Menéndez 2024). Each system exhibits distinct temporal and spatial signatures, which in combination define the seasonal wave climate of the region (Fig. 2 panel A to C, and Fig. 3).

The most persistent signal is associated with WS1, a swell-type regime generated in the Southern Ocean. WS1 dominates throughout the year, with daily presence above 90% at the three study sites, confirming its capacity to propagate over large distances into tropical latitudes (Portilla et al. 2015; Caicedo-Laurido et al. 2020). Its average Hs reaches a seasonal maximum in May, coinciding with the transition to the wet season and the weakening of the Panama Low-Level Jet (WS3). Conversely, WS1 exhibits lower Hs during the dry season (December–April), when WS3 is most active and propagates in the opposite direction.

WS2, linked to subtropical Pacific southerlies, is less persistent during the dry season, with monthly occurrence frequencies generally below 30%, but becomes more relevant during the wet season. During May–November, WS2 activity increases consistently across all study sites, with mean Hs values exceeding 0.4 m. This behavior reflects its swell-like characteristics, which favor energy conservation during long-distance propagation.

WS3, associated with the Panama Low-Level Jet (PLLJ), exhibits strong seasonality. Its maximum activity occurs during December–April, when it is present at up to 70% of days per month at sites 1 and 2. At site 3, however, the activity of WS3 is attenuated, likely due to the combined influence of the Pearl Islands Archipelago and the adjacent mountainous terrain of Darién, which limit the effect of this local wind system. A secondary but weaker activation of WS3 has been observed during El Niño years, particularly in July–August, with the signal being most evident during strong and very strong El Niño events (Rueda Bayona et al. 2007; Ordóñez-Zúñiga et al. 2021).

WS4 is controlled by the Chocó Low-Level Jet (ChLLJ), which flows northward along the Colombian Pacific and turns eastward toward Panama. Its seasonal cycle is tied to sea surface temperature gradients between the Niño 1+2 region and the Colombian Pacific (Sierra et al. 2018; Yepes et al. 2019). WS4 exhibits weaker activity from January to April, increasing markedly between May and December, with maximum intensity during September–November, when the ChLLJ reaches its northernmost extension. This pattern coincides with enhanced southwesterly winds during the northward shift of the Intertropical Convergence Zone (ITCZ).

Finally, WS5, associated with the northern storm belt of the North Extratropical Pacific, represents the least persistent system influencing the Gulf entrance. Its occurrence is constrained by both distance and local geographic barriers, generally producing Hs values below 0.50 m. Nevertheless, episodic extreme events generated by intense Northern Hemisphere storms can occasionally propagate into the

Table 1 Genesis and propagation directions of the identified WS in Fig. 2

Wave system	Incoming direction	Genesis
1	South–West	Southern Storm Belt—Extratropical—South Pacific
2	South–West	Southerlies—Subtropical—South Pacific
3	North	Local wind system—Panama Low Level Jet (PLLJ)
4	West	South Trade Winds—related to Chocó Low-Level Jet (ChLLJ)
5	West	Northern Storm Belt—Extratropical—North Pacific

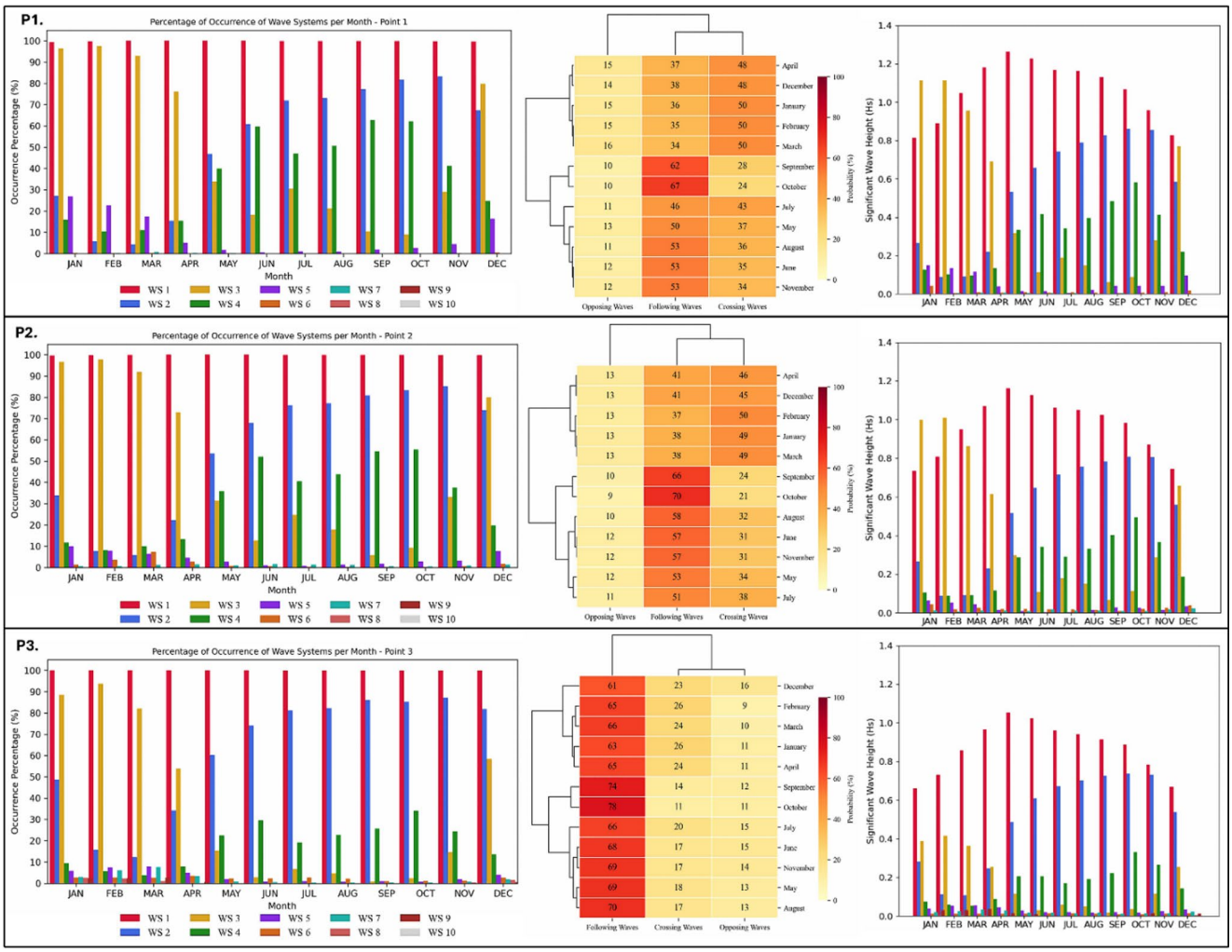

Fig. 3 Monthly median significant wave height (in meters) and probability of occurrence for each wave system, along with the categorization of wave types (Following, Crossing, Opposing) and their associated probabilities, based on wave spectrum data from 1969 to 2023, for each of the three study sites at the entrance to the Gulf of Panama

Gulf, producing transient increases in Hs at the study sites, with magnitudes depending on the intensity and trajectory of the originating storm (Amador et al. 2006).

3.2 Spatial modulation of wave systems by local geomorphology

The three study sites were strategically selected to capture the main geographic controls on wave propagation at the entrance of the Gulf of Panama (Fig. 1 panel A.2, and Fig. 2 panel D). Their comparison illustrates how large-scale forcing interacts with local bathymetric and orographic features, modulating the observed wave climate and the relative contribution of individual WS.

Site 1 (west side of the Gulf of Panama entrance) is directly influenced by the Azuero Peninsula, which acts as a partial barrier to the north-to-south propagating WS3 associated with the PLLJ. This geomorphological configuration deflects a portion of the incoming WS3 energy flux toward the southwest, generating a more complex and disordered

spectral signature. In contrast, southward-propagating swells (WS1, WS2, and WS4) are less affected by the peninsula and largely maintain their propagation into the Gulf, although some local attenuation and energy dispersion may occur. During the dry season (December–April), when WS3 becomes highly persistent, Site 1 records frequent crossing seas due to the interaction of the northeastward PLLJ-generated waves (WS3) with the southwestward swells of WS1. The frequency–direction spectra (Fig. 2, panel A to C) confirm this pattern, showing broader directional spreading and multiple energy peaks compared to the other sites. The effect is most evident during March–April, when WS3 peaks (> 70% of days active), while WS1 reaches its lowest mean Hs (< 0.35 m).

Site 2 (central side of the Gulf of Panama entrance) is minimally affected by coastal features and therefore exhibits wave conditions most representative of offshore (open-ocean) conditions. The temporal persistence of WS1 is systematically higher than at the other sites, with mean Hs values exceeding 0.4 m across most of the year, even during the dry season. Seasonal cycles are also more coherent with those reported in the Eastern Tropical Pacific, reinforcing the role of Site 2 as the most offshore-like reference within the Gulf. This coherence makes Site 2 a robust indicator of long-term variability, suitable for trend analysis and comparison across WS.

Site 3 (eastern side of the Gulf of Panama entrance) is a naturally sheltered location, receiving limited wave energy due to its position within the Gulf. Local features, such as the Pearl Islands Archipelago and the nearby Darién highlands, further attenuate waves from WS3, but the primary reason for low Hs values at this site is its enclosed geomorphological setting. As a result, locally generated waves (WS3) are significantly attenuated, with monthly persistence falling below 40% during the dry season, compared to ~ 70% at Sites 1 and 2. Similarly, WS4, although more active during the wet season, contributes less to the energy budget at Site 3 than at the other locations. The consequence is a systematic reduction of Hs across all systems at Site 3, with WS1 rarely exceeding 0.7 m during boreal winter months, due primarily to the semi-enclosed geomorphology that limits swell penetration.

A quantitative comparison across the three sites confirms these spatial contrasts. WS1 dominates year-round at all sites, but its mean Hs is consistently lower at Site 3 due to energy dissipation by geographic barriers. WS3 exhibits strong seasonal dependence, accounting for up to 70% of monthly occurrence at Sites 1 and 2 during December–April, while remaining substantially weaker at Site 3. WS2 and WS4 display parallel seasonal reinforcement during the ITCZ northward migration (May–November), but their energy contribution is again reduced at Site 3. In contrast, WS5 remains sporadic at all sites, with limited but occasionally extreme events capable of generating Hs > 0.5 m.

Correlation analyses further illustrate the interplay among systems (Fig. 4). WS1 and WS3 maintain strong negative correlations at all sites, reflecting their opposing seasonal cycles: when WS3 intensifies in boreal winter, WS1 reaches its lowest values. WS1 also correlates negatively with WS5, a relationship attributable to interhemispheric contrasts between boreal winter storm tracks and Southern Hemisphere low-pressure systems. In contrast, the positive correlation between WS3 and WS5 suggests regional atmospheric teleconnections, possibly linked to Atlantic–Pacific pressure gradients that promote simultaneous activity (Amador et al. 2006). Meanwhile, WS2 and WS4 show consistently strong positive correlations, confirming their shared dependence on ITCZ dynamics and their joint reinforcement during late boreal summer and early autumn.

Overall, these results highlight the complementary roles of the three study sites in characterizing the Gulf's wave climate. Site 2 captures the large-scale, offshore-like variability, consistently exhibiting higher mean Hs (> 0.4 m) year-round and coherence with regional Eastern Tropical Pacific patterns. Site 1 reflects local modulation by the Azuero Peninsula, showing increased directional spreading and frequent crossing seas during the dry season when WS3 is active, while Site 3 represents a naturally sheltered environment, with strongly attenuated Hs and reduced contributions from WS3 and WS4. Seasonal dynamics, such as the northward migration of the ITCZ, further reinforce differences among sites, affecting the relative persistence and intensity of WS2 and WS4. These observations confirm that all three sites can be jointly analyzed as representative wave nodes for the Gulf of Panama.

3.3 Temporal changes in wave system distributions and variance across periods

To explore temporal changes in the distribution and variability of WS at the Gulf of Panama entrance, Levene's test for variance and Mann–Whitney U tests for central tendency were applied across the three study periods (1969–1987, 1988–2005, 2006–2023) at each site. The results indicate statistically significant changes for most WS–site–season combinations. Levene's test commonly returned p-values < 0.01, confirming differences in variance, while Mann–Whitney U detected significant shifts in Hs medians ($p < 0.01$), indicating systematic changes in the distribution of wave heights (Figs. 5, 6).

WS1 (Southern Ocean swell) exhibited the most consistent changes. Variance differences were significant in nearly all comparisons ($p < 0.01$), except in a few cases affected by outliers, such as site 1 (1969–1987 vs. 1988–2005,

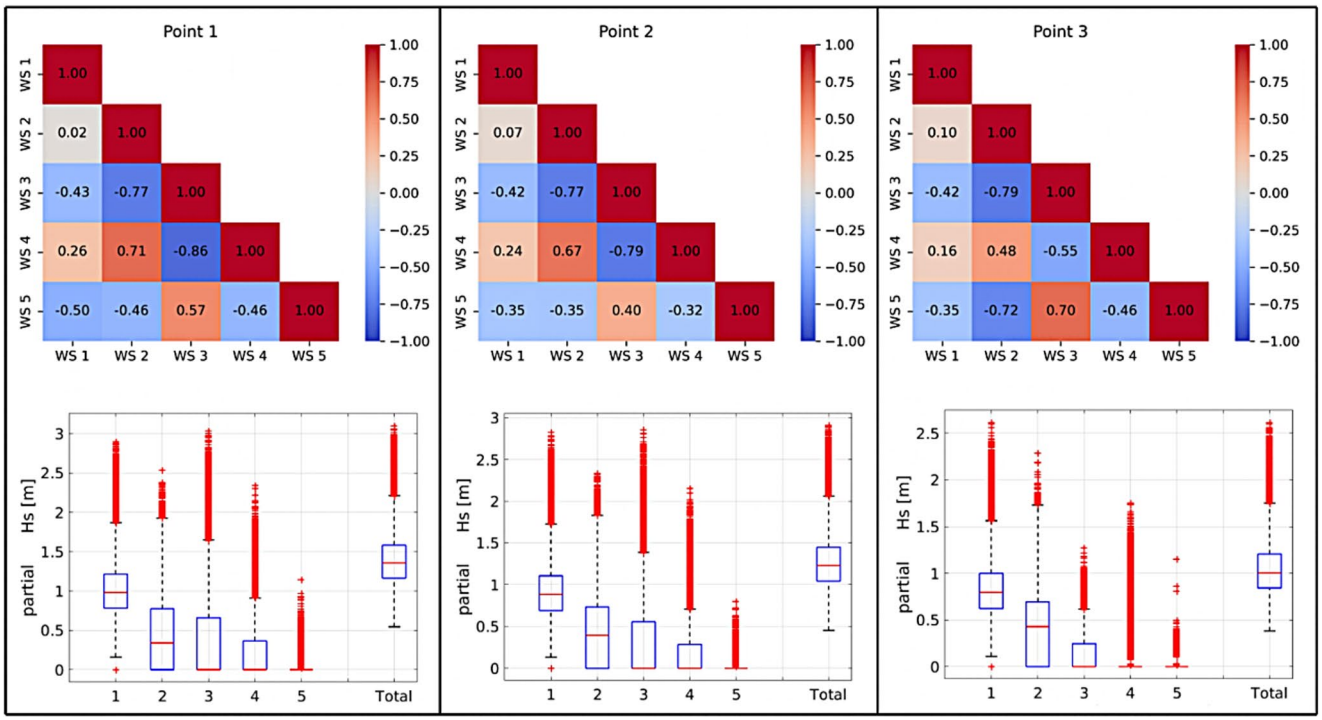

Fig. 4 Upper panel: Correlation analysis between the main WS at the study sites, based on the monthly averages of Hs from 1969 to 2023. Lower panel: partial Hs of the main WS identified the values representing the contribution of each system to the total sea state at the study site

$p > 0.05$) and select comparisons at site 2. Mann–Whitney U was significant in all site-period contrasts ($p < 0.01$). Mean dry-season Hs increased ≈0.05 m between 1969–1987 and 1988–2005, maintaining this increment into 2006–2023, while extreme Hs rose by more than 0.10 m across all sites. In the wet season, mean Hs increased ~0.05–0.10 m, with extremes increasing 0.08–0.13 m, resulting in progressively more frequent waves exceeding 2.00 m. These results align with projections for enhanced Southern Ocean swell events in the Eastern Pacific under RCP8.5 scenarios (Amores & Marcos 2020; Lemos et al. 2021; Semedo et al. https://doi.org/10.1175/JCLI-D-12-00658.12013).

WS2 (southerlies) also showed significant variance increases in almost all site–season comparisons (Levene $p < 0.01$) and significant shifts in median Hs (Mann–Whitney $p < 0.01$). Mean Hs increased by ~0.05–0.13 m between the baseline and later periods. Notable exceptions include site 1 (1988–2005 vs. 2006–2023) and site 3 (wet season), which remained relatively stable. The upper quartile (75th percentile) at sites 1–2 shifted from ~0.80–1.00 m (1969–1987) to ~1.00–1.25 m in later periods, reflecting a progressive increase in wave magnitudes. At site 3, the upper quartile remained < 1.00 m, with rare extremes > 1.5 m. Wet-season Hs mostly stayed below 1.00 m, but all late periods show upward displacement relative to the baseline. These trends are consistent with southerly wind-driven increases in wave energy in the subtropical South Pacific, with moderation at site 3 due to local coastal morphology (Odériz et al. 2021).

WS3 (PLLJ) exhibited strong temporal and spatial heterogeneity. Sites 1–2 experienced mean dry-season Hs increases of ≈0.11–0.16 m from 1969 to 1987 to 1988–2005, while increases in 2006–2023 were smaller (~0.06–0.09 m). Variance differences were significant (Levene $p < 0.01$), though some wet-season pairings at sites 1–2 (1988–2005 vs. 2006–2023) were non-significant. Extreme-value dispersion remained low (< 0.02 m), suggesting uniform upward shifts rather than increased variability. Site 3 consistently showed smaller Hs changes due to attenuation by the Pearl Islands and nearby highlands. Graphical analyses confirm that during the baseline dry season, sites 1–2 had frequent Hs < 1.00 m alongside extremes reaching 2.0–3.0 m, whereas later periods show elevated mean Hs and moderately increased extremes at site 3 (~0.07 m).

WS4 (ChLLJ) displayed significant variance changes in most comparisons (Levene $p < 0.01$), though some comparisons showed uniform mean shifts without variance increase (site 1: 1969–1987 vs. 1988–2005 dry season; site 2: 1969–1987 vs. 2006–2023 wet season). Mann–Whitney U confirmed central tendency differences ($p < 0.01$) except for sites 2–3 in the wet season of the two most recent periods. Mean Hs increased ≈0.06 m during the first transition period, with smaller changes (≤0.02 m) thereafter. Outlier

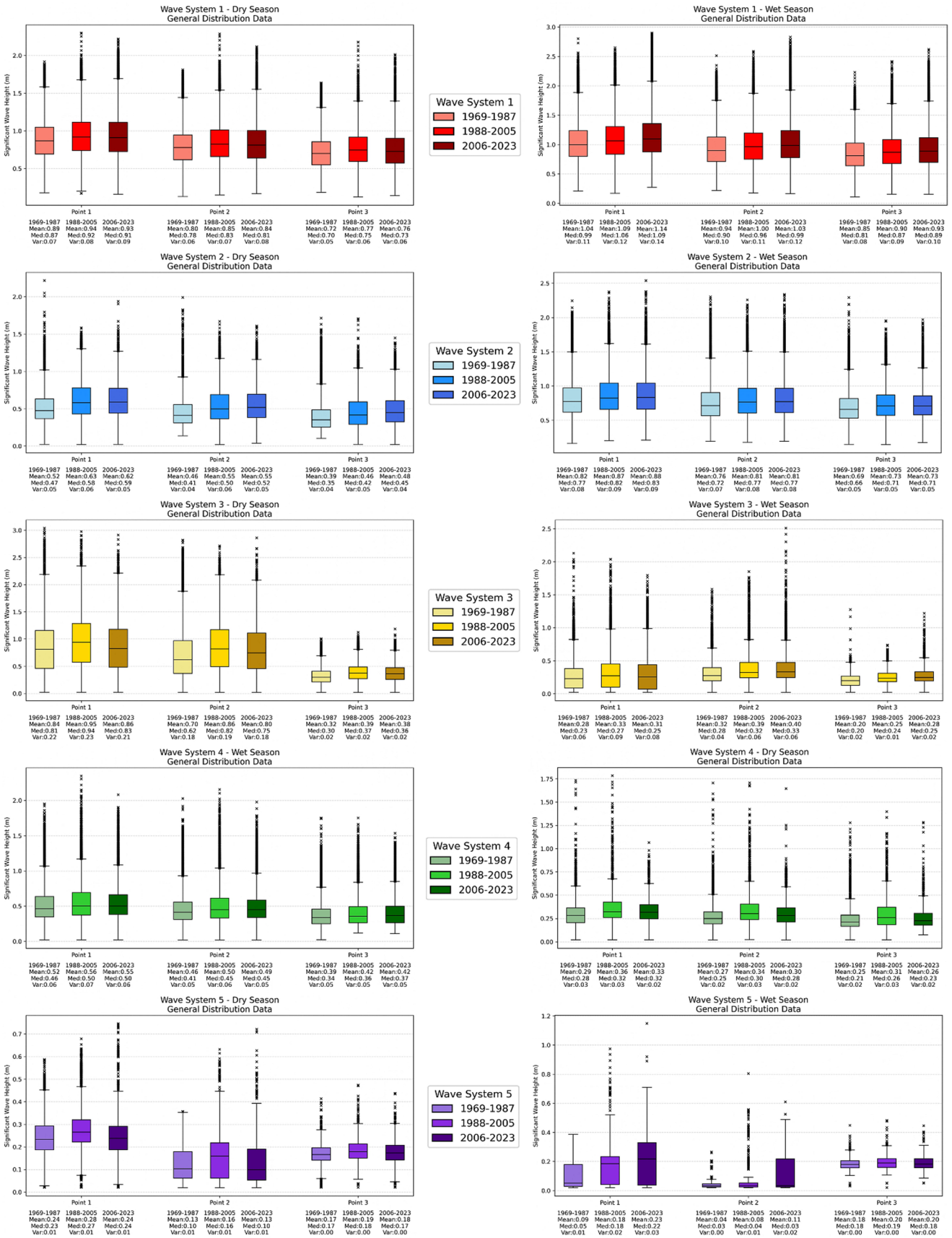

Fig. 5 Boxplot general data comparison for dry and wet season across the periods 1969–1987, 1988–2005, and 2006–2023

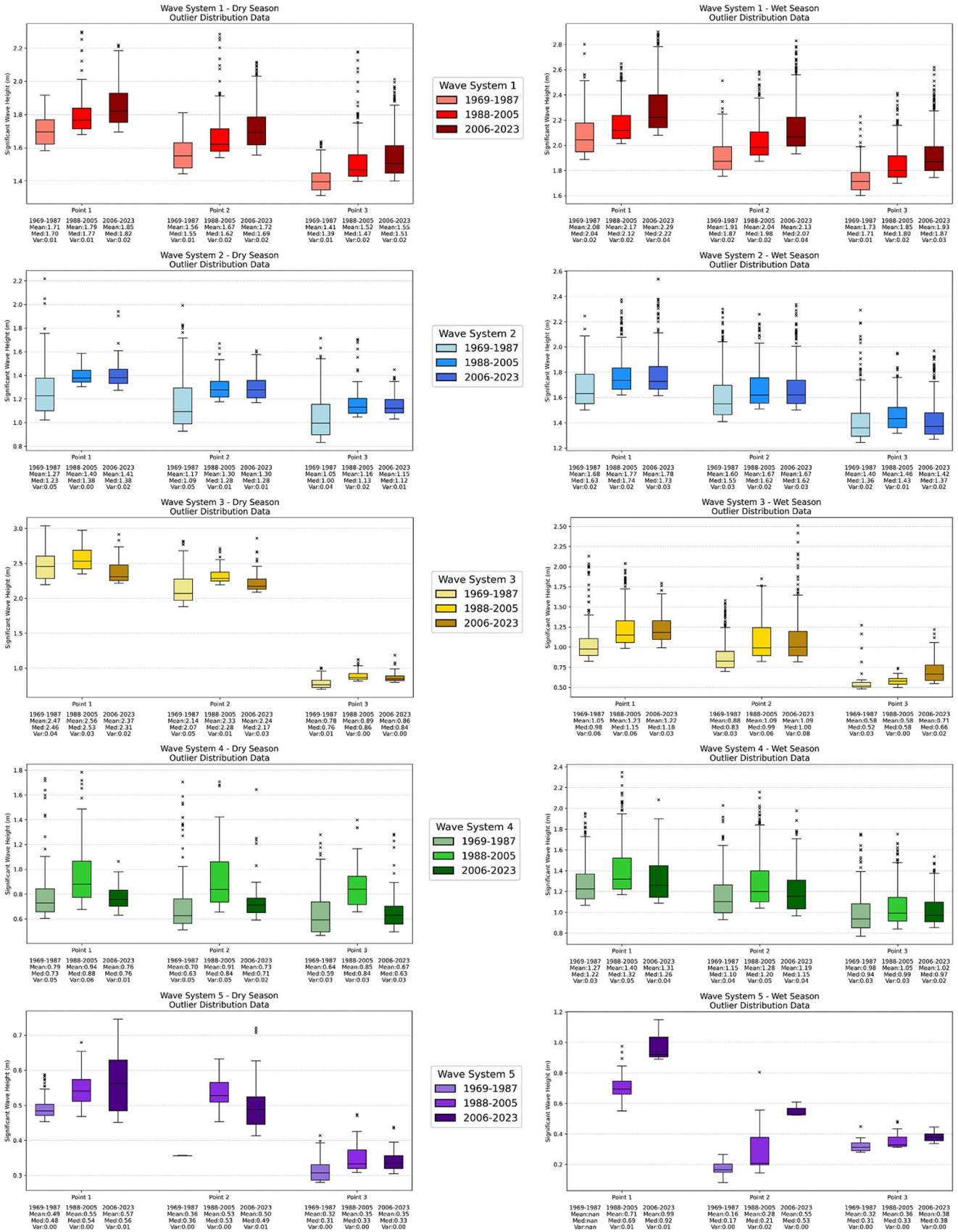

Fig. 6 Boxplot outliers data comparison for dry and wet season across the periods 1969–1987, 1988–2005, and 2006–2023

trends mirrored mean shifts, while site 3 showed an initial increase of ~0.11 m followed by a slight decrease in the latest period (dry season). These results are consistent with projected ChLLJ changes under RCP8.5 (Sierra et al. 2021).

WS5 (Northern Hemisphere storm belt) was highly episodic. Variance changes were non-significant at site 1 (dry season) and at site 3 (1988–2005 vs. 2006–2023). Mann–Whitney U detected significant distributional shifts in most comparisons ($p < 0.01$), except site 1 (1969–1987 vs. 2006–2023 dry season) and sites 2–3 (1988–2005 vs. 2006–2023 wet season). Exposure differed among sites: WS5-related waves occurred ~40% more frequently at site 1 than at sites 2–3, with site 3 being the least exposed. Changes in Hs were minor in the dry season (~0.01–0.03 m), while during the wet season, mean Hs increased by ~0.01–0.09 m. Interestingly, although extreme event frequency decreased at sites 1–2, mean Hs of those extremes increased by up to 0.28 m, indicating fewer but more energetic extreme waves.

3.4 Long-term trends in significant wave height (Hs) by percentile and system

Quantile regression analyses were conducted for the 50th and 95th percentiles of Hs, separated by season (dry vs. wet) and study period. All regressions were statistically significant (95% confidence level) and demonstrated relatively low standard errors. Positive trends were observed in both median and extreme Hs for most WS, with exceptions indicating non-uniform temporal changes. The resulting values represent the total change within each multi-decadal period, rather than annual rates. Results from these regressions are summarized in Table 2, which presents seasonal and site-specific changes (see Supplementary Materials for the Appendix).

Previous studies indicate that Hs in the Gulf of Panama has exhibited small but positive trends, typically ranging from 0 to 0.50 cm/yr over 1948–2008 (Reguero et al. 2013). Recent research highlights the importance of analyzing individual WS, as their contributions vary seasonally and can interact with ENSO events, emphasizing the multimodal nature of the Gulf's wave climate (Mazzaretto & Menendez 2024; Lobeto et al. 2022).

WS1 exhibited positive trends at the 50th percentile across all sites during 1969–1987, with mean Hs reaching > 0.05 m above baseline by the end of the period. The 95th percentile increased during wet seasons at all sites, while dry-season extremes decreased slightly at sites 2–3. For 1988–2005, the 50th percentile showed slight negative trends (~–0.05 m) in early months, while the 95th percentile reflected increased occurrence of Hs > 1.25 m. In 2006–2023, wet-season 50th percentile Hs increased > 0.10 m, while dry-season 95th percentile trends decreased (~–0.07 m), consistent with seasonal Southern Ocean swell patterns and previous regional studies (Reguero et al. 2019; Canavesio 2019; Godwyn-Paulson et al. 2020; Zheng et al. 2022a).

WS2 and WS4 showed higher interannual variability in the dry season. WS2 50th percentile waves > 0.40 m increased during 1969–1987 at all sites, whereas WS4 increases were mostly > 0.20 m at sites 2–3. In 1988–2005, dry-season 50th percentile trends increased (WS2: > 0.45 m; WS4: moderate increases) and 95th percentile trends reflected extreme waves up to 1.25 m. Wet-season trends were similar, though extreme WS4 events were irregular. In 2006–2023, both WS2 and WS4 decreased in most sites, especially in late dry-season periods, reflecting ENSO-modulated variability (Romero-Centeno et al. 2007; Sierra et al. 2018; Yepes et al. 2019; Torres et al. 2022).

WS3 displayed positive dry-season trends > 0.05 m at sites 1–2 during 1969–1987, weaker influence at site 3. The 95th percentile increased for waves > 1.50 m at sites 1–2 and > 0.50 m at site 3. Later periods showed reduced dry-season extremes, consistent with decreased positive ENSO events. Wet-season increases were smaller due to lower WS3 activity, though some coincided with prolonged ENSO-positive years (Ordóñez-Zúñiga et al. 2021; Torres et al. 2022).

WS5 exhibited irregular trends, with dry-season waves slightly increasing in 1969–1987 at sites 1–2, while wet-season trends were more heterogeneous. Site 3 remained largely stable. Observed patterns are consistent with projected reductions in Northern Hemisphere swell propagation under RCP8.5 (Amores & Marcos 2020; Lemos et al. 2021; Zheng et al. 2022b).

3.5 Variability of peak wave period (Tp) and extreme conditions in the Gulf of Panama

Figure 7 illustrates clear seasonal cycles in Tp across all five WS and highlights modest but system-dependent changes between the three analysis periods (1969–1987, 1988–2005 and 2006–2023). Overall, the dominant pattern is a strong intra-annual signal, with each system displaying a characteristic timing of maxima and minima, which is superimposed on smaller inter-period shifts whose sign and magnitude vary by system and by site. Visual inspection indicates the most coherent recent increases in Tp occur in WS1 (particularly during the wet season) and in parts of WS4, whereas WS2 and WS3 are generally stable or show slight reductions and WS5 is spatially heterogeneous with no single directional trend across sites.

WS1 shows the strongest and most coherent temporal variations, with Tp following a well-defined annual cycle characterized by early-year minima and sustained maxima during the wet season (June–October). Compared with

Table 2 Trends derived from quantile regression: total changes in Hs (cm) for the 50th and 95th percentiles within each multi-decadal period, based on dry- and wet-season data at each study site

Quantile	Year	Season	Study area	WS1 Trend cm	WS2 Trend cm	WS3 Trend cm	WS4 Trend cm	WS5 Trend cm
0.50	1969–1987	Dry	Site 1	9.42	4.30	15.05	−2.18	7.96*
			Site 2	6.93	2.78	14.93	1.70	12.36*
			Site 3	5.53	2.64	5.67	0.96	1.21*
		Wet	Site 1	8.51	−8.45	−0.32	−10.21	3.16*
			Site 2	8.70	−9.17	0.98	−8.84	0.60*
			Site 3	8.80	−9.82	−0.51	−6.04	2.00*
	1988–2005	Dry	Site 1	−11.39	17.23	13.86	3.97	0.73*
			Site 2	−12.76	13.68	29.75	4.49	8.85*
			Site 3	−13.30	7.68	8.19	3.56	2.16*
		Wet	Site 1	−4.99	9.73	11.37	14.63	0.82*
			Site 2	−6.14	10.13	9.10	13.50	0.41*
			Site 3	−6.84	9.33	6.10	10.87	−1.55*
	2006–2023	Dry	Site 1	5.77	−6.56	−0.45	−1.23	−1.70*
			Site 2	3.01	−4.02	−0.42	−3.78	−7.89*
			Site 3	2.39	−1.19	1.23	−2.01	−1.03*
		Wet	Site 1	14.71	−4.08	−0.88	−2.98	7.12*
			Site 2	12.77	−3.86	0.10	−3.75	0.99*
			Site 3	11.42	−1.06	−2.00	−2.28	0.42*
0.95	1969–1987	Dry	Site 1	2.10	5.64	9.05	0.51	8.94*
			Site 2	−0.34	5.34	10.45	−10.90	8.12*
			Site 3	−2.21	0.58	6.77	−5.21	−0.65*
		Wet	Site 1	3.53	−28.85	11.75	−31.32	1.24*
			Site 2	1.43	−25.98	3.83	−39.79	5.47*
			Site 3	1.18	−21.14	5.15	−48.01	2.61*
	1988–2005	Dry	Site 1	−7.30	10.73	6.60	15.18	−18.18*
			Site 2	−5.39	17.79	20.23	39.69	−32.20*
			Site 3	−4.54	13.63	9.41	39.55	7.47*
		Wet	Site 1	−4.33	8.37	56.00	36.21	54.34*
			Site 2	−1.36	5.45	31.74	38.47	28.35*
			Site 3	2.49	6.17	11.87	37.57	3.01*
	2006–2023	Dry	Site 1	−6.94	−19.01	−5.52	−9.75	1.98*
			Site 2	−9.02	−19.43	−1.98	−25.67	8.54*
			Site 3	−10.70	−13.49	2.31	−19.82	3.15*
		Wet	Site 1	14.91	−10.11	−12.55	−13.46	4.29*
			Site 2	15.53	−9.10	−18.95	−17.11	50.76*
			Site 3	15.60	−8.02	−16.90	−19.59	14.31*

*The trends presented are not fully representative of the wave system due to its high temporal variability during the period analyzed

1988–2005, the most recent period (2006–2023) shows higher Tp values in many of the wet-months, with typical increases on the order of ~ 0.3–0.6 s; relative to the baseline period (1969–1987) the recent periods are commonly ~ 0.4–0.6 s larger across much of the year. Because these Tp increases coincide with previously observed increases in Hs for WS1, the joint change in Hs and Tp points to an increase in wave energy during the wet season. Such a shift has plausible geomorphological and hazard implications (elevated nearshore energy is likely to increase sediment mobilization and the potential for coastal erosion and flooding during high tides or storms), but these consequences must be quantified together with local bathymetry, tidal context, and storm statistics.

WS4 displays a more complex, site-dependent signal. All sites show pronounced early-year peaks (Feb–Mar) and larger month-to-month variability than WS1. Sites 1 and 2 present moderate increases in Tp during August–October in both 1988–2005 and 2006–2023 compared with 1969–1987, with differences visually on the order of ~ 0.3–0.8 s, while site 3 shows larger inter-period scatter and less coherence. This pattern suggests that at least part of the observed change for WS4 is spatially localized and likely controlled by exposure and wave incidence angle; where increases are

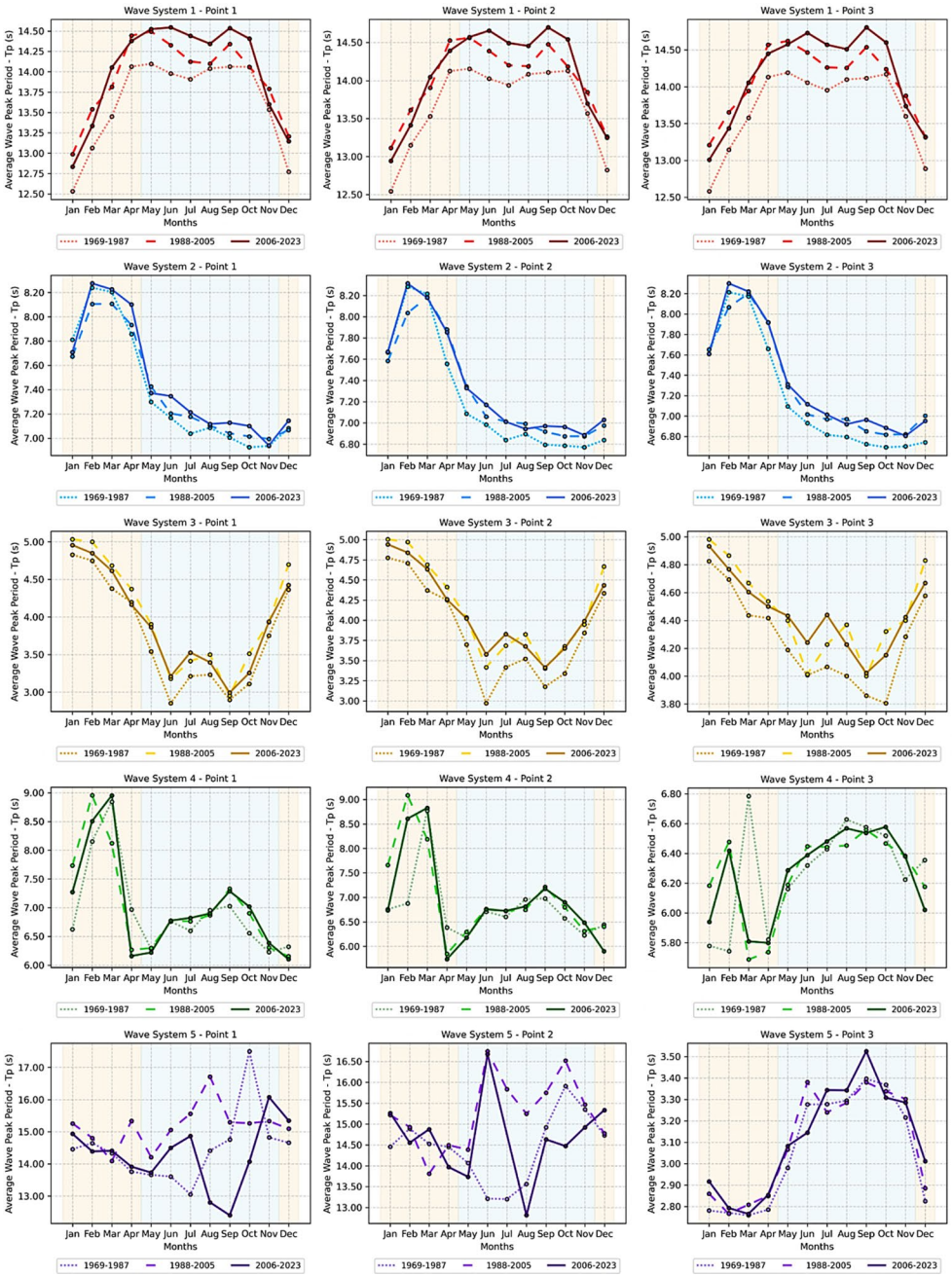

Fig. 7 Temporal variability of the average monthly Tp across the periods 1969–1987, 1988–2005, and 2006–2023 for the different WS at the three study sites. The shading in the background highlights the seasonal cycle, the dry season (December–April) and the wet season (May–November)

temporally collocated with coastal impact events, they may contribute to episodic intensifications of coastal hazard.

By contrast, WS2 and WS3 do not show consistent or sustained increases in Tp across the study area. WS2 reaches its highest Tp early in the year (Jan–Mar, near 8 s) and then gradually declines toward mid-year. The baseline period (1969–1987) often contains some of the larger monthly Tp values, while month-to-month differences between periods remain modest (typically < 0.8 s). WS3 exhibits the lowest Tp among the WS (3.0–5.0 s) and shows only minor differences between periods (generally < 0.5 s), indicating stable temporal behavior.

WS5 stands apart because its changes are neither large nor spatially uniform. In some months and sites, Tp decreased in 2006–2023 compared with 1969–1987 by nearly 1 s, whereas in other months the values increased or remained almost unchanged. The variability in both sign and magnitude across sites and months prevents the identification of a coherent region-wide trend. This high spatial heterogeneity limits the possibility of drawing strong generalizations about recent changes in this system based solely on the plotted series.

In summary, the evidence suggests that changes in Tp within the Gulf of Panama are system-specific and have

different implications for coastal dynamics. The most consistent increases, observed in WS1 during the wet season and parts of WS4, imply that recent decades have been characterized by waves of longer period coinciding with the season when coastal flooding and erosion events are more frequent. Longer-period waves carry more energy shoreward and enhance sediment mobilization, thereby increasing the potential for shoreline retreat and damage to coastal infrastructure, particularly in low-lying areas where tidal ranges already exceed 4.00 m. In contrast, the relative stability of WS2 and WS3, and the spatially heterogeneous behavior of WS5, indicate that not all systems contribute equally to long-term changes in coastal forcing. Overall, the evidence points to an emerging scenario in which wet-season conditions in the Gulf of Panama are gradually shifting toward higher-energy wave climates, with direct consequences for erosion potential, coastal flooding, potentially affecting the long-term resilience of natural and human systems along the gulf's shoreline.

3.5.1 Extreme wave characteristics: analysis of events exceeding the 99th percentile

The analysis of Hs and Tp values exceeding the 99th percentile provides critical insights into the behavior of the five primary WS (i.e., WS1–WS5) in the Gulf of Panama and their potential implications for coastal hazards. Across both dry and wet seasons and all study periods (1969–1987, 1988–2005, 2006–2023), variability in extreme Hs consistently exceeds that of Tp, reflecting the higher sensitivity of wave amplitude to local and regional atmospheric forcing, whereas Tp remains relatively stable even during severe events (Tables 3, 4). Notably, Tp occasionally exceeds characteristic seasonal values during extreme episodes, indicating the influence of long-traveling swell and episodic wind-driven waves on coastal dynamics.

WS1 (Southern Ocean swell) dominates both the frequency and magnitude of extreme events throughout the year (Lemos et al. 2019). For events exceeding the 99th percentile, Hs at Sites 1–2 typically ranges from 2.0 m to 3.0 m, with Tp between 16 s and 20 s, sustained for approximately 48 h, particularly during the wet season. These extreme conditions are the primary causes of coastal impacts, including erosion and inundation. The propagation direction of WS1 is predominantly north-northeast (20°–40°), facilitating effective energy transmission into the Gulf entrance. During the dry season, extreme Hs decreases to ~ 1.7 m–2.0 m, with slightly shorter periods (Tp 14 s–20 s), illustrating the seasonally modulated energy contribution of this system (Fig. 8). WS2, WS3 (PLLJ), and WS4 (ChLLJ) exhibit comparatively stable extreme-event characteristics. Extreme Hs for these systems rarely exceeds 1.5 m, and Tp remains near baseline seasonal values, suggesting predictable coastal impacts. WS2 contributes moderate but persistent energy flux during peak wind periods, while WS3 and WS4 are more seasonally and spatially variable but generally produce smaller extremes than WS1. Their cumulative effect, however, may still influence shoreline adjustments and sediment transport, particularly during the wet season when multiple systems reinforce wave energy simultaneously (Romero-Centeno et al. 2007; Sierra et al. 2018; Yepes et al. 2019).

WS5, associated with North Pacific hurricanes and tropical cyclones, is highly episodic. Although Hs typically remains below 1.0 m, these events can deliver long-period

Table 3 Average Hs and Tp for events exceeding the 99th percentile during the dry season

Season/year	Study area	WS1 Hs mean (m) Tp mean (s)	WS2 Hs mean (m) Tp mean (s)	WS3 Hs mean (m) Tp mean (s)	WS4 Hs mean (m) Tp mean (s)	WS5 Hs mean (m) Tp mean (s)
Dry 1969–1987	Site 1	1.71 m 15.32 s	1.45 m 6.88 s	2.38 m 6.73 s	1.09 m 7.09 s	0.52 m 17.27 s
	Site 2	1.58 m 15.35 s	1.42 m 6.58 s	2.16 m 6.62 s	1.10 m 6.93 s	0.33 m 16.34 s
	Site 3	1.42 m 15.26 s	1.27 m 6.57 s	0.79 m 6.25 s	1.00 m 7.10 s	0.34 m 2.90 s
Dry 1988–2005	Site 1	1.81 m 15.79 s	1.45 m 6.66 s	2.33 m 6.71 s	1.31 m 5.87 s	0.61 m 13.23 s
	Site 2	1.70 m 15.95 s	1.40 m 6.47 s	2.16 m 6.57 s	1.26 m 5.99 s	0.58 m 13.63 s
	Site 3	1.56 m 16.06 s	1.22 m 6.82 s	0.88 m 5.95 s	1.12 m 6.35 s	0.41 m 3.14 s
Dry 2006–2023	Site 1	1.91 m 16.37 s	1.42 m 6.63 s	2.19 m 6.52 s	0.86 m 6.87 s	0.66 m 12.51 s
	Site 2	1.79 m 16.37 s	1.36 m 6.63 s	2.07 m 6.45 s	0.89 m 6.83 s	0.59 m 13.93 s
	Site 3	1.62 m 16.29 s	1.17 m 6.63 s	0.85 m 5.91 s	0.92 m 6.36 s	0.37 m 2.97 s

Table 4 Average Hs and Tp for events exceeding the 99th percentile during the wet season

Season/year	Study area	WS1 Hs mean (m) Tp mean (s)	WS2 Hs mean (m) Tp mean (s)	WS3 Hs mean (m) Tp mean (s)	WS4 Hs mean (m) Tp mean (s)	WS5 Hs mean (m) Tp mean (s)
Wet 1969–1987	Site 1	2.16 m 16.18 s	1.83 m 7.20 s	1.36 m 5.27 s	1.52 m 6.63 s	0.32 m 15.53 s
	Site 2	1.97 m 16.13 s	1.76 m 7.07 s	1.19 m 5.25 s	1.45 m 6.85 s	0.22 m 13.74 s
	Site 3	1.75 m 15.92 s	1.53 m 7.06 s	0.65 m 5.09 s	1.30 m 6.77 s	0.38 m 3.31 s
Wet 1988–2005	Site 1	2.20 m 16.57 s	1.87 m 7.34 s	1.58 m 5.83 s	1.68 m 6.66 s	0.85 m 11.33 s
	Site 2	2.09 m 16.64 s	1.77 m 7.23 s	1.53 m 5.83 s	1.59 m 6.86 s	0.60 m 11.73 s
	Site 3	1.90 m 16.60 s	1.53 m 7.31 s	0.64 m 5.70 s	1.36 m 6.88 s	0.44 m 3.49 s
Wet 2006–2023	Site 1	2.41 m 17.02 s	1.89 m 7.27 s	1.45 m 5.63 s	1.57 m 6.45 s	0.92 m 11.17 s
	Site 2	2.24 m 17.20 s	1.78 m 7.16 s	1.60 m 5.86 s	1.46 m 6.56 s	0.54 m 11.17 s
	Site 3	2.01 m 17.08 s	1.53 m 7.28 s	0.95 m 6.09 s	1.27 m 6.61 s	0.42 m 3.24 s

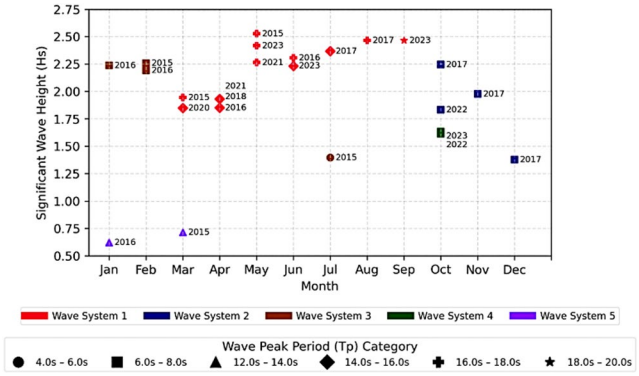

Fig. 8 Monthly averages of Hs events lasting more than 12 h and the average Tp, derived from the 99th percentile of data from study site 1, from 2015 onward

waves to Sites 1–2, contributing disproportionately to energy flux and potential coastal stress. Propagation directions for WS5 range from northeast to southeast (80°–120°), with local geomorphology, particularly the Pearl Islands and highlands near Site 3, attenuating wave energy before reaching enclosed areas. The "Pali hurricane" of January 2016 exemplifies this behavior, generating Hs of 0.6 m–0.7 m and Tp of 12 s–14 s at the southern Gulf boundary, coinciding with the 2014–2016 positive ENSO phase (Morris & Sabia 2016; Steenkamp et al. 2019). This demonstrates how ENSO-modulated atmospheric and oceanic anomalies can extend the spatial reach of Northern Hemisphere storm-driven waves.

Seasonality strongly modulates extreme-event characteristics. Wet-season extremes exhibit both higher Hs and longer Tp compared to dry-season events, reflecting the influence of long-traveling Southern Ocean swell and coincident regional wind-driven systems. Documented high-impact events, such as May 2015 and September 2023, illustrate compound hazard scenarios, with sustained Hs of 2.0 m–3.0 m and Tp of 16 s–20 s persisting for ~ 48 h, causing significant damage to coastal infrastructure (Cavaleri et al. 2022; Godwyn-Paulson et al. 2020). In contrast, dry-season extremes, while still impactful, are less energetic and generally produce minor inundation without major structural damage.

Overall, this analysis highlights that extreme waves in the Gulf of Panama are primarily driven by WS1, with secondary contributions from WS2–WS4 and episodic WS5 events. The distinct seasonal patterns, combined with spatial modulation by local geomorphology, emphasize the need to account for both amplitude and period in hazard assessments, particularly when planning for compound events or ENSO-related anomalies.

3.6 ENSO-driven variability in wave systems

The influence of ENSO on the Gulf of Panama wave climate is evident in both median and extreme Hs, yet its impact varies across WS, seasons, and study periods (1969–1987, 1988–2005, 2006–2023; see Fig. 10). Correlation analyses using the Niño 3.4 index reveal coherent positive Hs anomalies during La Niña for most systems (Fig. 9), whereas El Niño predominantly amplifies the Panama Low-Level Jet (WS3) and generates contrasting responses for Southern Ocean swell (WS1) and other WS (Torres et al. 2022; Portilla-Yandún et al. 2016).

During La Niña, southern swell-dominated conditions (WS1) intensify, particularly in the wet season

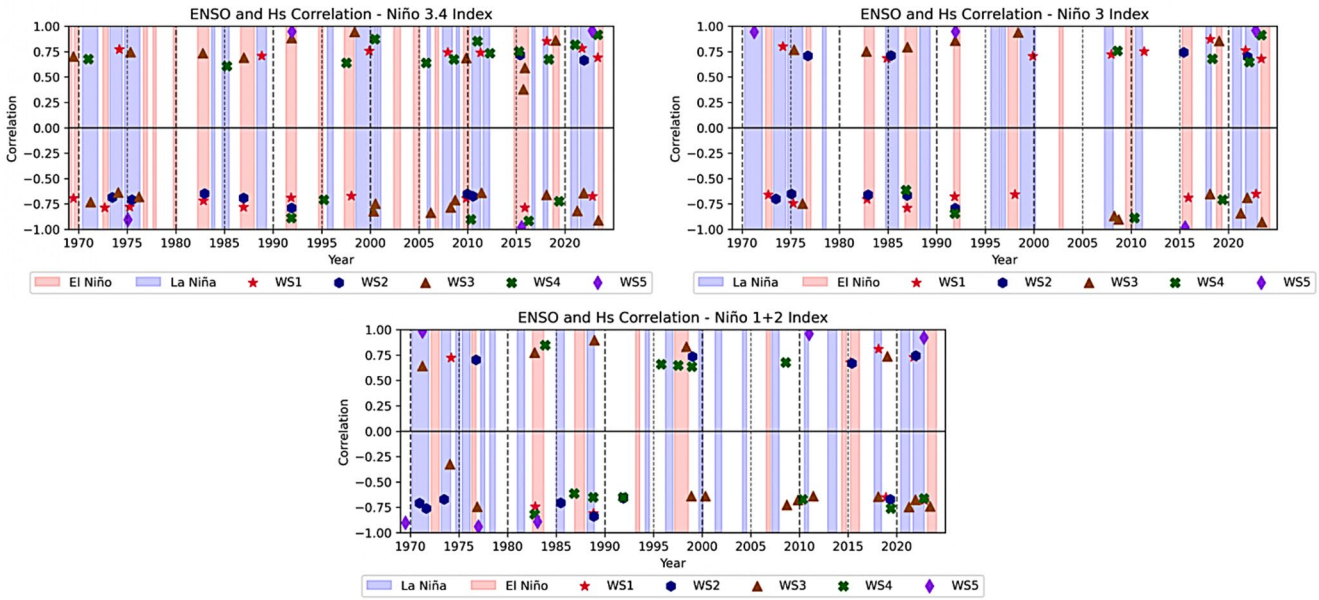

Fig. 9 Correlation results between the monthly variability of Hs from WS (data above 50th percentile) and the anomalies recorded for ENSO indices. This analysis uses 10 months (WS1, WS2, WS3 and WS4) and 5 months (WS5) sliding window correlations for the complete data period from 1969 to 2023

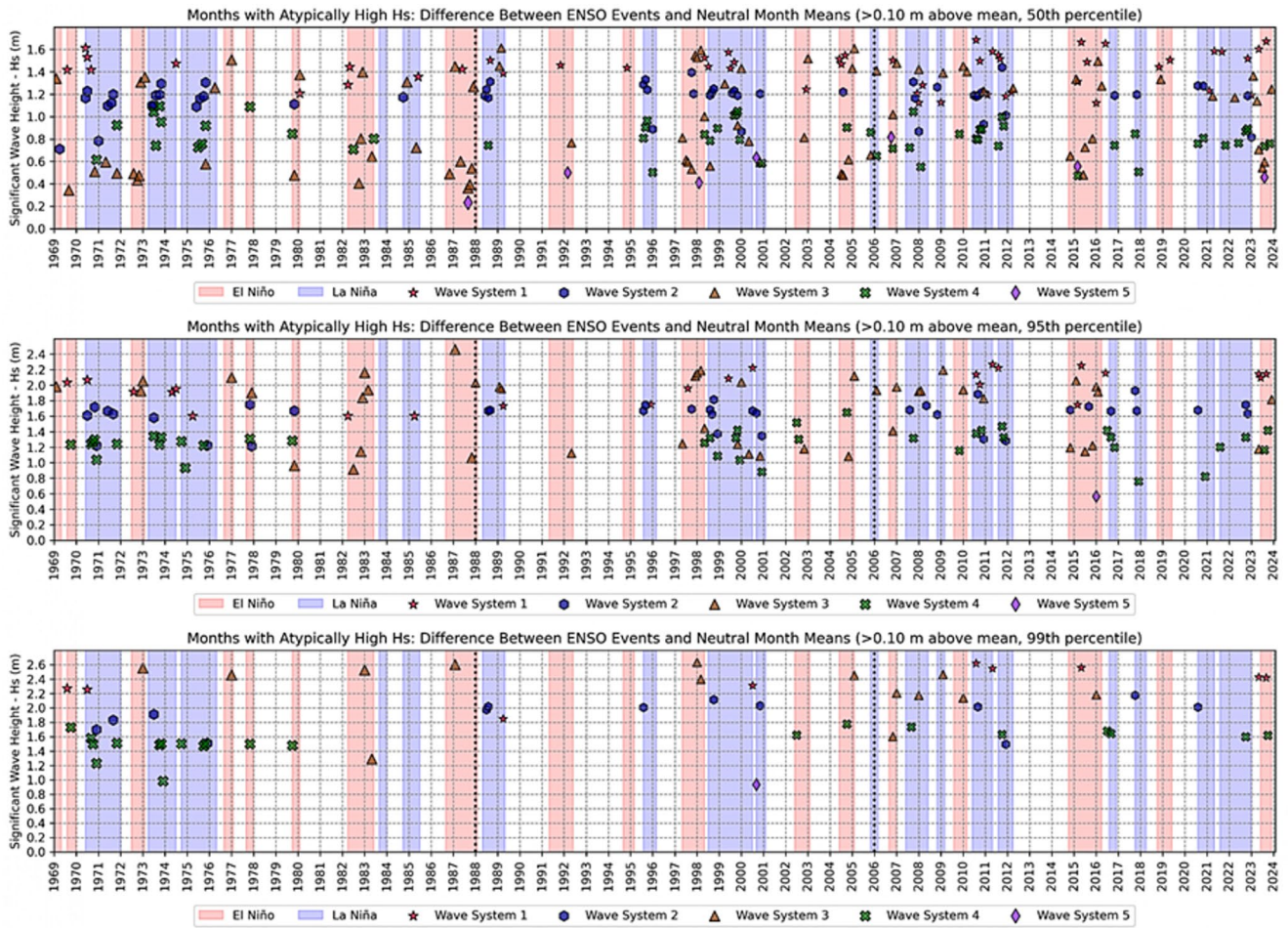

Fig. 10 Months with positive Hs anomalies exceeding 0.10 m during ENSO events (identified using the Niño 3.4 index), determined by the difference with neutral months for the 50th, 95th, and 99th percentiles

(May–November). Monthly anomalies above the 50th percentile indicate increases exceeding 0.10 m in Hs during 2006–2023, compared with modest reductions (<0.10 m) in earlier periods (1969–2005). This pattern reflects strengthened southerly wind fetches in the Eastern Tropical Pacific, delivering higher wave energy into the Gulf (Aramburo et al. 2022). Exceptional El Niño events, such as May 2015 and September 2023, produced local positive Hs anomalies up to 0.25 m and 0.15 m, respectively, illustrating that extreme events can depart from typical ENSO-driven tendencies (Cavaleri et al. 2022; Godwyn-Paulson et al. 2020). At the 95th and 99th percentiles, ENSO correlations are less consistent, highlighting the dominant influence of episodic storms and tropical cyclones on extreme Hs.

Mid-latitude and regional WS (i.e., WS2 and WS4) show a subtler but coherent ENSO signal. While WS2 exhibits minimal dry-season variation, wet-season anomalies reveal modest Hs decreases during El Niño (May–November) and increases exceeding 0.10 m during La Niña. WS4, linked to the Chocó Low-Level Jet, similarly intensifies under La Niña due to enhanced trade winds along the Pacific coast of South America, producing Hs increases above 0.10 m from August to November in 1988–2023 (Sierra et al. 2021; Cerón et al. 2021). These seasonal enhancements corroborate previous observations that regional LLJs respond sensitively to ENSO-driven large-scale wind anomalies, with implications for wet-season wave energy and nearshore sediment transport.

WS3 (PLLJ) displays a distinct ENSO response, with strong positive correlations during El Niño. Dry-season Hs increases exceed 0.10 m at the 50th percentile, reflecting intensified jet activity and associated local wind-wave generation, whereas La Niña tends to slightly suppress Hs. At higher percentiles (95th–99th), January consistently shows increased Hs, aligning with the peak of dry-season PLLJ activity and El Niño teleconnections (Mori et al. 2013). The interaction between WS3 and WS1 during El Niño amplifies crossing seas at exposed Gulf sites, potentially enhancing extreme coastal impacts.

Northern Hemisphere storm-driven waves (WS5) demonstrate a highly episodic ENSO response, with strong El Niño events (e.g., 1982, 1997, 2016) facilitating southward swell propagation into the equatorial Pacific and producing notable dry-season Hs peaks (Zhang et al. 2023). Conversely, La Niña events exert minimal influence due to weakened SST-driven atmospheric circulation, and percentile-based analyses indicate inconsistent correlations, reflecting the stochastic nature of storm-driven extremes (Aramburo et al. 2022).

Overall, ENSO emerges as a key modulator of Gulf of Panama wave climate at interannual scales, influencing both seasonal and extreme Hs. Positive La Niña phases generally elevate wet-season wave heights, while El Niño amplifies dry-season LLJ-driven systems. Yet, the dominance of extreme events and episodic storm activity, particularly at the 95th and 99th percentiles, complicates direct attribution, underscoring the necessity of percentile-based approaches to understand ENSO-wave linkages and their implications for coastal hazards.

4 Discussion

4.1 Multi-scale drivers of wave climate variability and site-specific modulation

The variability and spatial distribution of the five WS at the entrance of the Gulf of Panama result from a complex interplay between large-scale atmospheric drivers and local geomorphological constraints. WS1 represents the dominant year-round regime, yet its effective contribution to coastal wave energy varies substantially across the Gulf due to site-specific factors. Its peak mean Hs in May coincides with the attenuation of WS3 activity, reflecting the seasonal weakening of the PLLJ (Rueda Bayona et al. 2007; Ordóñez-Zúñiga et al. 2021). Conversely, during the dry season, WS1 interacts antagonistically with the intensified WS3, resulting in frequent crossing seas at Site 1 and Site 2, which are evident in both directional spectra and increased directional spreading (Portilla et al. 2015; Caicedo-Laurido et al. 2020).

WS2 and WS4, display coherent seasonal patterns reinforced by the northward migration of the ITCZ (García et al. 2009; Portilla et al. 2015; Sierra et al. 2018). Their positive correlation across sites shows a shared dependence on these large-scale atmospheric features, with energy maxima during the wet season (May–November). However, the influence of local bathymetry and orography modulates their contribution to the coastal energy budget. At Site 3, a semi-enclosed and sheltered environment, both WS4 and WS5 are attenuated compared to Sites 1 and 2, highlighting how local geomorphology constrains the propagation of incident waves. Similarly, the Pearl Islands Archipelago and the highlands of Darien reduce the persistence of WS3 at Site 3 (see Fig. 2 and Fig. 3), despite its high activity at the western and central sites, demonstrating that geomorphological features selectively filter the effect of atmospheric forcing (Rueda Bayona et al. 2007; Mora 2018; Caicedo-Laurido et al. 2020).

WS5 remains sporadic but can episodically generate Hs values (>0.5 m) across the Gulf, contributing to extreme events (Amador et al. 2006). Its positive correlation with WS3 suggests that boreal winter atmospheric teleconnections and Atlantic–Pacific pressure gradients may synchronize the activity of Northern Hemisphere storm-driven

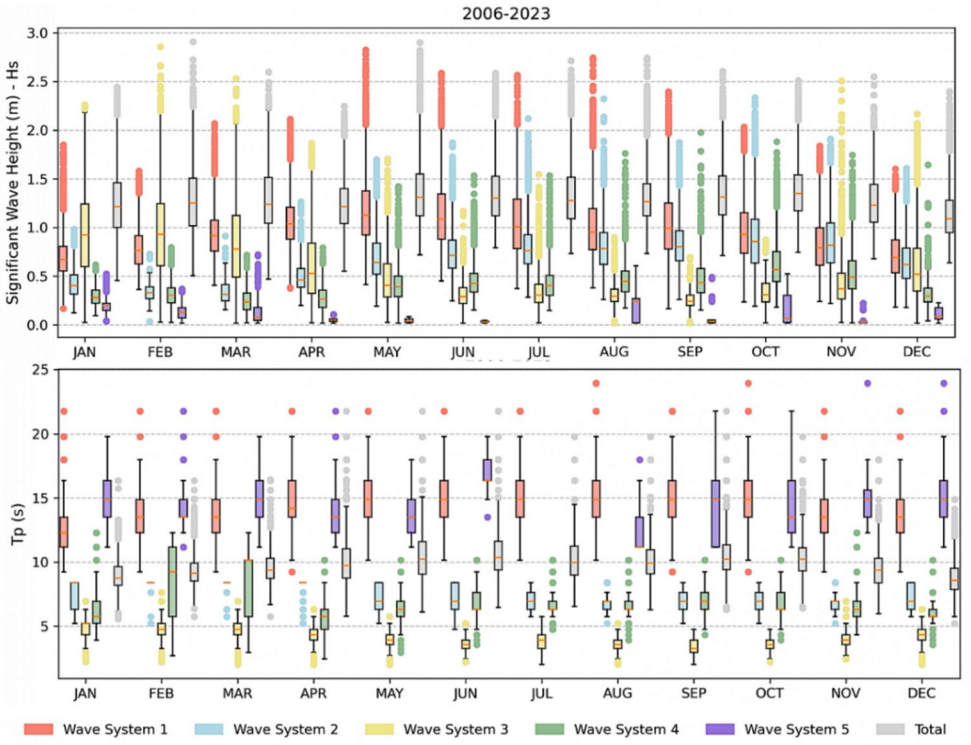

Fig. 11 Comparison of monthly Hs and Tp for each Wave System vs. Total values at study site 2 (period 2006–2023)

waves with locally forced systems. In contrast, WS1 correlates negatively with WS3 and WS5, reflecting the interhemispheric opposition of Southern and Northern Hemisphere storm systems and the seasonal alternation of dominant wave regimes (Amador et al. 2006; Portilla et al. 2015).

The combined effect of these interactions has direct implications for coastal dynamics. At Site 1 and Site 2, frequent following waves and coincident peaks of WS1, WS2, and WS4 during September–October enhance wave energy reaching the shoreline, coinciding with documented episodes of coastal flooding and erosion (Romero-Centeno et al. 2007; Sierra et al. 2021). The spatial variation among sites emphasizes the influence of local modulating features: the Azuero Peninsula at Site 1 redirects energy fluxes, leading to disordered wave patterns; Site 2 exhibits offshore-like conditions, providing a robust representation of regional wave variability; and Site 3 remains sheltered, with lower Hs values and reduced contributions from WS3 and WS4. These dynamics suggest that risk assessments and coastal management strategies must account for both the temporal concurrence of WS and the spatial heterogeneity imposed by bathymetric and orographic features (Portilla-Yandún, 2018; IH-Cantabria 2021).

Moreover, the observed seasonal and inter-system correlations provide a mechanistic framework to interpret coastal impacts beyond simple univariate wave statistics. The inverse relationship between WS1 and WS3 explains periods of reduced Hs at the western and central Gulf during the dry season, whereas the synchronous reinforcement of WS2 and WS4 during the wet season amplifies the energy flux toward the coast. Extreme WS5 events, though rare, act as additional drivers of episodic flooding and erosion, underscoring the need to consider compound wave events in future hazard assessments (Amador et al. 2006; Sierra et al. 2021). Understanding these multi-scale interactions is critical for improving predictive models of coastal response and for guiding the implementation of monitoring and early-warning systems tailored to the Gulf of Panama's unique environmental setting.

In addition, resolving variability at the level of individual WS rather than through bulk wave parameters provides an essential complement to this physical interpretation. As illustrated in Fig. 11, total Hs and Tp may appear relatively stable even when individual systems undergo substantial seasonal or interannual fluctuations, due to compensatory effects among WS1–WS5. These hidden contributions highlight the limitations of integrated metrics and the value of spectral decomposition for identifying system-specific drivers, crossing-sea conditions, and the timing of extreme events. This system-based perspective is particularly relevant for multimodal wave climates in the eastern tropical Pacific, where direction–frequency spectral analyses allow the identification of concurrent wave systems generated by local winds (sea) and by distant storms (swell). In regions such as the Gulf of Panama, the temporal overlap of these systems produces complex and variable sea states that are not adequately represented by bulk parameters,

underscoring the importance of resolving individual wave systems to properly characterize coastal wave conditions.

4.2 Implications of long-term Hs trends for coastal dynamics and hazard assessment

The long-term trends observed in Hs across the Gulf of Panama have substantial implications for coastal dynamics and hazard assessment, particularly when considering the distinct behavior of each wave system (WS1–WS5), site-specific responses, and temporal evolution across the study periods (1969–1987, 1988–2005, 2006–2023).

WS1 exhibits systematic and pervasive increases in both mean and extreme Hs, particularly pronounced during the wet season. Quantile regression analyses reveal that median Hs at the 50th percentile increased progressively by over 0.05 m at all sites during the early period, with the 95th percentile reflecting heightened extremes during austral winter months (Reguero et al. 2019; Canavesio 2019; Godwyn-Paulson et al. 2020). These increases in swell events contribute to greater wave energy flux along the Gulf's entrance, enhancing coastal stress during peak months and amplifying the potential for shoreline erosion, flooding, and sediment transport. Notably, site-specific modulation is evident: Sites 1 and 2, more exposed to offshore swell propagation, experienced larger increases in extreme Hs (up to > 2.0 m), whereas the semi-sheltered Site 3 displayed lower Hs and reduced variability, highlighting the protective role of geomorphological features such as the Pearl Islands and nearby highlands (Portilla et al. 2015; Caicedo-Laurido et al. 2020).

WS2 and WS4 display consistent wet-season increases in median and upper-quartile Hs, particularly at the western and central Gulf sites. Increases in the 75th percentile from approximately 0.80–1.00 m to 1.00–1.25 m at Sites 1–2 indicate a progressive shift toward higher wave magnitudes over successive periods. In contrast, Site 3 exhibits an attenuated signal, with median and extreme values rarely exceeding 1.0 m, underscoring the role of local coastal morphology in attenuating incoming wave energy. These trends imply that even modest increases in offshore-generated waves can induce differential impacts across the Gulf, with exposed areas experiencing heightened flooding risk and accelerated erosion rates, particularly during the wet season when WS2 and WS4 act synergistically with WS1 to elevate coastal wave energy (Odériz et al. 2021; Romero-Centeno et al. 2007; Sierra et al. 2018; Yepes et al. 2019).

WS3 demonstrates pronounced temporal and spatial heterogeneity. Dry-season Hs increases of ≈0.11–0.16 m were recorded at Sites 1–2 during the transition from the baseline period to 1988–2005, followed by smaller increases (~0.06–0.09 m) in 2006–2023. Variance analyses indicate that extreme-value dispersion remained low, suggesting that extremes shifted upward without becoming more variable. The combination of higher mean and extreme Hs during the dry season, coinciding with persistent WS3 activity, promotes frequent crossing seas when interacting with WS1, particularly in the western Gulf. Such interactions amplify peak wave energy, enhancing the potential for localized sediment mobilization and episodic shoreline inundation (Ordóñez-Zúñiga et al. 2021; Torres et al. 2022). At Site 3, geomorphological shielding produced attenuated increases, underscoring how semi-enclosed environments can buffer regional wind-driven wave enhancements and reduce local coastal hazards.

WS5 presents highly episodic behavior but with important implications for extreme events. Although variance changes were generally minor or non-significant at Sites 1 and 3, Mann–Whitney U tests revealed significant shifts in Hs distributions at most site–period combinations. Interestingly, while the frequency of extreme WS5 events decreased at the more exposed western and central sites, the mean Hs of these extremes increased by up to 0.28 m. This indicates that episodic but more energetic storm-driven waves may act as primary drivers of extreme coastal events, even if their occurrence is sporadic, emphasizing the need to incorporate compound wave events into hazard modeling and coastal planning (Amores & Marcos 2020; Lemos et al. 2021; Zheng et al. 2022b).

The long-term trends observed, including positive shifts in median and extreme Hs across multiple WS, translate directly into elevated coastal risk. Sites 1 and 2, with greater exposure, are subject to increased energy fluxes that can exacerbate beach erosion, destabilize nearshore sediment budgets, and elevate the likelihood of inundation during compound events. Conversely, Site 3, despite experiencing smaller absolute changes, remains sensitive to extreme WS1 and WS2 events due to the semi-enclosed nature of its setting, which can trap wave energy and enhance local runup during high-magnitude swells. Furthermore, differences in the timing and strength of WS peaks across seasons highlight the need to analyze multiple WS, since the simultaneous occurrence of WS1–WS4 during the wet season can strongly amplify coastal impacts.

4.2.1 Extreme events and percentile-based analysis

The analysis of wave events exceeding the 99th percentile provides a focused perspective on the most severe episodes capable of generating coastal impacts in the Gulf of Panama. Extreme events, defined by Hs and Tp values above the 99th percentile, reveal that variability in Hs is substantially greater than that of Tp, indicating that wave amplitude responds more strongly to episodic atmospheric and swell forcing than wave period, which remains relatively stable

across seasons and study periods. These observations are particularly relevant for understanding the potential coastal hazards associated with each WS and the differential exposure of each study site.

During wet-season, WS1 produces the most extreme events, with Hs ranging from 2.0 m to 3.0 m and Tp between 16 s and 20 s, sustained for approximately 48 h. These conditions coincide with documented impacts on coastal infrastructure, such as the May 2015 and September 2023 events, which caused damage to housing and commercial establishments across Site 1 and Site 2 (Cavaleri et al. 2022; Godwyn-Paulson et al. 2020). Dry-season extremes were slightly lower (Hs 1.7 m–2.0 m; Tp 14 s–20 s), producing minor inundation without significant structural damage. The propagation direction of WS1 (20º–40º NNE) facilitates effective energy transmission across the Gulf, while semi-enclosed features, including the Pearl Islands and highlands, reduce Hs at Site 3, demonstrating the importance of geomorphological modulation on extreme event impacts.

WS5 produces fewer extreme Hs events but can propagate long-period waves to Site 1 and Site 2, although their amplitudes remain relatively low (< 1.0 m). Notable cases include the "Pali hurricane" of January 2016, characterized by Hs 0.6 m–0.7 m and Tp 12 s–14 s, linked to anomalously warm SST and the positive ENSO phase of 2014–2016 (Morris & Sabia 2016; Steenkamp et al. 2019). Although WS5 extremes are infrequent, their long-period energy contributes to coastal stress, especially when coinciding with elevated WS1 or WS2 activity.

WS2, WS3, and WS4 show relatively stable extreme Hs and Tp values across seasons and study periods. WS3 and WS4 rarely exceed 1.5 m in Hs, with Tp closely tracking seasonal averages, and their combined effect contributes to steady wave-driven sediment transport rather than episodic inundation. WS2 exhibits a comparable pattern, though wet-season Hs can reach slightly higher magnitudes (~ 1.2 m at Sites 1–2). This stability across space and time provides a more predictable influence on coastal morphology, supporting reliable hazard assessments and management planning in the Gulf of Panama.

Seasonal modulation is evident across all systems. Wet-season extremes consistently present higher Hs and longer Tp, reflecting the combined influence of Southern Ocean swells, subtropical southerlies, and regional Low-Level Jets (LLJ). The co-occurrence of WS1–WS4 peaks during May–November can amplify wave energy fluxes, particularly at exposed Sites 1 and 2, producing non-linear effects on shoreline erosion and inundation. These patterns emphasize the critical role of percentile-based analysis in linking long-term trends with actual coastal impacts, as extreme Hs and Tp values provide a mechanistic explanation for observed episodes of damage and local flooding, complementing median- and quartile-based assessments.

Finally, the alignment of extreme event occurrence with ENSO phases suggests a strong teleconnection between large-scale climatic variability and local coastal hazards. Positive and negative ENSO events modulate the frequency, height, and period of extreme Hs episodes, particularly for WS1 and WS5, highlighting the importance of integrating climate teleconnections into hazard prediction and coastal management frameworks (Cavaleri et al. 2022; Godwyn-Paulson et al. 2020; Morris & Sabia 2016). This underscores the need for continued monitoring of extreme events and percentile-based analyses to support robust risk assessment and the design of mitigation strategies tailored to site-specific exposure and geomorphology.

4.3 ENSO modulation of coastal wave climate

The influence of ENSO on the Gulf of Panama's wave climate manifests as a complex interplay between large-scale ocean–atmosphere variability and site-specific geomorphological constraints. Analysis of monthly Hs anomalies relative to the Niño 3.4 index reveals that La Niña phases are generally associated with enhanced wave heights at the 50th percentile for WS1 and WS4, particularly during the wet season (May–November), whereas El Niño conditions primarily amplify WS3 activity during the dry season. These correlations, however, diminish for the 95th and 99th percentiles, where extreme events driven by episodic storm systems or tropical cyclones dominate, reflecting the stochastic nature of the highest-energy events (Aramburo et al. 2022; Torres et al. 2022; Sierra et al. 2021).

During La Niña, WS1 exhibits positive Hs anomalies exceeding 0.10 m in 2006–2023 across almost all months, particularly during the wet season. By contrast, in earlier periods (1969–1987, 1988–2005), La Niña events produced smaller or negligible changes in Hs (< 0.10 m) between October and February, illustrating an inter-period intensification of La Niña influence. This increase is consistent with strengthened southerly winds in the tropical South Pacific, generating higher swell energy that propagates northward into the Gulf of Panama while concurrently decreasing Northern Hemisphere contributions (Aramburo et al. 2022; Cavaleri et al. 2022). Notably, exceptional El Niño events, such as May 2015 and September 2023, produced Hs anomalies of up to 0.25 m and 0.15 m, respectively, associated with prolonged (~ 48 h) high-energy conditions (Hs 2.0 m–3.0 m; Tp 16 s–20 s), which resulted in significant impacts on coastal communities and infrastructure (Godwyn-Paulson et al. 2020; Cavaleri et al. 2022). These cases exemplify departures from the general La Niña–dominant pattern and underscore the importance of integrating event

duration and persistence when assessing ENSO-driven hazards.

WS3 displays a contrasting ENSO response. Positive correlations with Hs are primarily observed during El Niño, particularly in dry-season months at Sites 1–2, where 50th percentile anomalies exceed 0.10 m and 95th percentile extremes reach > 1.50 m. Conversely, La Niña slightly reduces Hs (< 0.10 m). This ENSO-driven modulation explains periods of frequent crossing seas when WS3 coincides with WS1, amplifying wave energy flux at the western Gulf, which can lead to episodic sediment mobilization and localized shoreline inundation (Ordóñez-Zúñiga et al. 2021; Torres et al. 2022). Site 3, by contrast, demonstrates attenuated responses due to geomorphological shielding, highlighting the differential translation of regional ENSO-forced wave energy into local coastal hazards.

ENSO modulation also affects WS2 and WS4, with wet-season Hs increasing by more than 0.10 m during La Niña, particularly at Sites 1–2. These changes reflect the intensification of regional trade winds, which enhance both subtropical southerlies and the Chocó Low-Level Jet (Sierra et al. 2021; Cerón et al. 2021). At Site 3, sheltered conditions limit these increases, with median and extreme Hs rarely exceeding 1.0 m, illustrating how local geomorphology attenuates ENSO-driven wave energy. While the absolute magnitudes of these anomalies are smaller than those of WS1 or WS3, the cumulative effect over successive wet-season months contributes to coastal energy flux and gradual shoreline displacement, particularly when high WS1 activity or episodic WS5 events coincide.

WS5 exhibits highly variable behavior due to the stochastic nature of extratropical and tropical storm activity. Strong El Niño events (1982, 1997, 2016) drove southward-propagating North Pacific swells that produced dry-season Hs peaks at the exposed western Gulf sites (Zhang et al. 2023). By contrast, La Niña phases had minimal influence, as weakened SST-driven circulation limited both the frequency and intensity of these swells. Site-specific exposure further modulates impacts, with Sites 2–3 experiencing smaller effects due to their relative sheltering, highlighting the challenges in predicting extreme WS5 events.

5 Conclusions

The analysis of the Gulf of Panama's wave climate reveals a complex interplay between local geomorphology, regional atmospheric circulation, and large-scale oceanic drivers, producing a multimodal coastal wave regime characterized by distinct seasonal and interannual variability. The dominant WS (i.e., WS1–WS5) exhibit differentiated behavior: WS1 (Southern Ocean swells) persists year-round with the highest contribution to coastal wave energy, while WS2 and WS4 (southern-origin swells and Chocó Low-Level Jet-driven waves) intensify during the wet season, generating increased wave energy from the south-southwest. WS3, associated with the Panama Low-Level Jet, displays an inverse relationship with these southern systems, producing crossing seas that amplify wave complexity and sediment mobilization. WS5, influenced by extratropical Northern Hemisphere storms, contributes sporadically under extreme conditions, reflecting the stochastic nature of episodic storm-driven swells.

Local geomorphology exerts a major control on wave exposure and energy distribution. The Azuero Peninsula and Pearl Islands Archipelago induce site-specific modulation of Hs and Tp, with Site 2 reflecting offshore-like wave spectra, Site 1 experiencing higher seasonal variability, and Site 3 benefiting from semi-enclosed protection, leading to reduced Hs and more stable wave periods. These findings emphasize the necessity of accounting for geomorphic shielding in coastal hazard assessments and wave energy evaluations.

Long-term analyses across 1969–2023 reveal increasing trends in Hs and the frequency of extreme waves, particularly during the wet season. WS1 exhibits a steady rise in both median and extreme Hs, corresponding to enhanced Southern Ocean swell propagation. WS2 and WS4 show coordinated seasonal peaks linked to large-scale wind patterns, while WS3 activity intensifies during El Niño and diminishes under La Niña or neutral conditions. Although WS5 remains episodic, its extremes have increased in magnitude over recent decades. These trends suggest that ongoing changes in atmospheric circulation and global wave climate are reinforcing Southern Hemisphere swell contributions while altering the influence of regional wind-driven systems, with direct consequences for coastal erosion, flooding, and sediment transport.

Wave period (Tp) variations complement Hs trends, reflecting shifts in spectral composition. WS1 exhibits longer Tp during wet-season extremes, amplifying coastal inundation potential, while WS2 and WS4 contribute to combined swell and local wind-sea interactions. WS3 Tp remains relatively stable except during strong El Niño events, and WS5 Tp shows high interannual variability consistent with episodic storm inputs. The integration of Hs and Tp underscores the value of spectral analyses in capturing energy and period dynamics critical for hazard assessment.

ENSO phases emerge as a key modulator of interannual wave variability. La Niña is generally associated with positive anomalies in WS1 and WS4, particularly during the wet season, whereas El Niño predominantly enhances WS3 during the dry season. Extreme events (95th–99th percentiles), however, are primarily driven by episodic storms

and tropical cyclones, highlighting the system-dependent and stochastic nature of the highest-energy waves. Notably, exceptional events such as May 2015 and September 2023 illustrate the combined influence of ENSO and prolonged high-energy conditions, resulting in significant coastal impacts.

The results of this work highlight the value of analyzing wave climate variability through individual WS. A system-based spectral perspective provides information that is not captured by bulk parameters, offering a clearer view of the processes driving seasonal patterns, long-term changes, and episodic high-energy events. This approach enhances the characterization of multimodal wave climates and supports more informed assessments of coastal dynamics and potential hazards in the Gulf of Panama.

It is important to emphasize that the present study relies primarily on reanalysis data from numerical models, as long-term in-situ wave measurements in the Gulf of Panama are unavailable. While ERA5 provides a comprehensive dataset, it is worth noting that the number and type of observations assimilated have increased over time, which may introduce temporal variations in data coverage and accuracy. Consequently, the results presented here should be interpreted as the best approximation currently attainable, highlighting the need for future field campaigns to obtain direct measurements. Such observations would help validate model-based findings, reduce uncertainties, and improve the understanding of local wave dynamics.

Supplementary Information The online version contains supplementary material available at https://doi.org/10.1007/s00382-025-08007-w.

Acknowledgements The authors express their gratitude to the Centro de Modelización Matemática en Áreas Clave para el Desarrollo (MODEMAT) at the Escuela Politécnica Nacional in Quito-Ecuador, for providing access to the GLOSWAC-5 dataset. Ruby Vallarino-Castillo expresses her gratitude to the University of Panama for its support to the project " Explorando la evolución de nuestras costas: estudio de la erosión costera y su impacto en las comunidades locales, frente a horizontes de emergencia climática", also extends her gratitude to the Secretaría Nacional de Ciencias, Tecnología e Innovación (SENACYT) of Panama for the financial support provided through Grant APY-NI-2024A-02.

Data availability Graphical indicators from GLOSWAC-5 are freele available at https://gloswac.epn.edu.ec/, datasets can be obtained under request.

Declarations

Conflict of interest The authors declare no conflict of interest.

References

Amador JA (2008) The Intra-Americas Sea low-level jet: Overview and future research. In: Annals of the New York Academy of Sciences. Blackwell Publishing Inc., pp 153–188

Amador JA, Alfaro EJ, Lizano OG, Magaña VO (2006) Atmospheric forcing of the eastern tropical Pacific: a review. Prog Oceanogr 69:101–142. https://doi.org/10.1016/j.pocean.2006.03.007

Amores A, Marcos M (2020) Ocean swells along the global coastlines and their climate projections for the twenty-first century. J Clim. https://doi.org/10.1175/JCLI-D-19

Aramburo D, Montoya RD, Osorio AF (2022) Impact of the ENSO phenomenon on wave variability in the Pacific Ocean for wind sea and swell waves. Dyn Atmos Oceans. https://doi.org/10.1016/j.dynatmoce.2022.101328

Bundschuh J, Alvarado GE (2012) Coastal morphology and coral reefs. In: Central America: Geology, Resources and Hazards, 1st Edition. CRC Press, London

Caicedo-Laurido AL, Torres-Parra RR, Orfila-Förster A, Tobar-Mosquera CA (2020) Variabilidad estacional del oleaje sea y swell en la Cuenca Pacífica Colombiana. In: Compilación Oceanográfica de la Cuenca Pacífica Colombiana II. Editorial Dimar, pp 134–152

Calil J, Reguero BG, Zamora AR, Losada IJ, Méndez FJ (2017) Comparative Coastal Risk Index (CCRI): A multidisciplinary risk index for Latin America and the Caribbean. PLoS ONE. https://doi.org/10.1371/journal.pone.0187011

Canavesio R (2019) Distant swells and their impacts on atolls and tropical coastlines. The example of submersions produced by lagoon water filling and flushing currents in French Polynesia during 1996 and 2011 mega swells. Glob Planet Change 177:116–126. https://doi.org/10.1016/j.gloplacha.2019.03.018

Cavaleri L, Benetazzo A, Bertotti L, Bidlot JR, Pomaro A, Portilla-Yandun J (2022) The 2015 exceptional swell in the Southern Pacific: generation, advection, forecast and implied extremes. Prog Oceanogr. https://doi.org/10.1016/j.pocean.2022.102840

Cerón WL, Kayano MT, Andreoli RV, Avila-Diaz A, de Souza IP, Souza RAF (2021) Pacific and atlantic multidecadal variability relations with the choco and caribbean low-level jets during the 1900–2015 period. Atmosphere. https://doi.org/10.3390/atmos12091120

Davison S, Benetazzo A, Barbariol F, Ducrozet G, Yoo J, Marani M (2022) Space-time statistics of extreme ocean waves in crossing sea states. Front Mar Sci. https://doi.org/10.3389/fmars.2022.1002806

Donelan MA, Drennan WM, Katsaros KB (1997) The air-sea momentum flux in conditions of wind sea and swell. J Phys Oceanogr. https://doi.org/10.1175/1520-0485(1997)027%3c2087:TASMFI%3e2.0.CO;2

Gastwirth JL, Gel YR, Miao W (2009) The Impact of Levene's Test of Equality of Variances on Statistical Theory and Practice. Statistical Science

Godwyn-Paulson P, Jonathan MP, Hernandez FR, Muthusankar G, Lakshumanan C (2020) Coastline variability of several Latin

American cities alongside Pacific Ocean due to the unusual "Sea Swell" events of 2015. Environ Monit Assess. https://doi.org/10.1007/s10661-020-08469-x

Grimaldo MA (2014) Plano de las olas del Golfo de Panamá. Tecnociencia (Panama) 16

Hao L, Naiman D (2007) Quantile Regression. SAGE Publications, Inc., 2455 Teller Road, Thousand Oaks California 91320 United States of America

Hasselmann S, Brüning C, Hasselmann K, Heimbach P (1996) An improved algorithm for the retrieval of ocean wave spectra from synthetic aperture radar image spectra. J Geophys Res 101(C7):16615–16629. https://doi.org/10.1029/96JC00798

Hegermiller CA, Rueda A, Erikson LH, Barnard PL, Antolinez JAA, Mendez FJ (2017) Controls of multimodal wave conditions in a complex coastal setting. Geophys Res Lett 44:12,315-12,323. https://doi.org/10.1002/2017GL075272

Holthuijsen L (2007) Waves in Oceanic and Coastal Waters. Waves in Oceanic and Coastal Waters, by Leo H Holthuijsen, pp 404 Cambridge University Press, January 2007 ISBN-10: ISBN-13: https://doi.org/10.2277/0521860288

Hoogervorst C (2022) Unravelling sediment transport driven by a multimodal wind-wave spectrum. Master's thesis, Delft University of Technology. Available at: https://resolver.tudelft.nl/uuid:fa4d3279-3443-41bc-a995-6d81f34d6936

Instituto de Hidráulica Ambiental—Universidad de Cantabria (IH Cantabria) (2021) Development of a marine dynamics database for the Panamanian coasts to assess vulnerability and climate change impacts to sea level rise

Instituto de Hidráulica Ambiental—Universidad de Cantabria (IH Cantabria), Comisión Económica para América Latina y el Caribe (CEPAL) (2015) Efectos del cambio climático en la costa de América Latina y el Caribe - Impactos

Kirezci E, Young IR, Ranasinghe R, Muis S, Nicholls RJ, Lincke D, Hinkel J (2020) Projections of global-scale extreme sea levels and resulting episodic coastal flooding over the 21st Century. Sci Rep. https://doi.org/10.1038/s41598-020-67736-6

Lemos G, Semedo A, Dobrynin M, Behrens A, Staneva J, Bidlot JR, Miranda PMA (2019) Mid-twenty-first century global wave climate projections: results from a dynamic CMIP5 based ensemble. Glob Planet Change 172:69–87. https://doi.org/10.1016/j.gloplacha.2018.09.011

Lemos G, Semedo A, Hemer M, Menendez M, Miranda PMA (2021) Remote climate change propagation across the oceans—the directional swell signature. Environ Res Lett. https://doi.org/10.1088/1748-9326/ac046b

Levene, H. (1960) Robust tests for equality of variances. Contributions to Probability and Statistics: Essays in Honor of Harold Hotelling, Stanford University Press, pp 278–292

Lincke D, Hinkel J, Mengel M, Nicholls RJ (2022) Understanding the Drivers of Coastal Flood Exposure and Risk From 1860 to 2100. Earths Futre. https://doi.org/10.1029/2021EF002584

Lira-Loarca A, Besio G (2022) Future changes and seasonal variability of the directional wave spectra in the Mediterranean Sea for the 21st century. Environ Res Lett 17:104015. https://doi.org/10.1088/1748-9326/ac8ec4

Lobeto H, Menendez M, Losada IJ, Hemer M (2022) The effect of climate change on wind-wave directional spectra. Glob Planet Change. https://doi.org/10.1016/j.gloplacha.2022.103820

Losada IJ, Reguero BG, Méndez FJ, Castanedo S, Abascal AJ, Mínguez R (2013) Long-term changes in sea-level components in Latin America and the Caribbean. Glob Planet Change 104:34–50. https://doi.org/10.1016/j.gloplacha.2013.02.006

Luijendijk A, Hagenaars G, Ranasinghe R, Baart F, Donchyts G, Aarninkhof S (2018) The State of the World's Beaches. Sci Rep. https://doi.org/10.1038/s41598-018-24630-6

Mazzaretto OM, Menendez M (2024) A worldwide coastal analysis of the climate wave systems. Front Mar Sci. https://doi.org/10.3389/fmars.2024.1385285

McKnight PE, Najab J (2010) Mann-Whitney U Test. The Corsini encyclopedia of psychology. https://doi.org/10.1002/9780470479216.corpsy0524

Mora G (2018) Climatology of the low-level winds over the intraamericas sea using satellite and reanalysis data. Tópicos meteorológicos y oceanográficos

Mori N, Shimura T, Yasuda T, Mase H (2013) Multi-model climate projections of ocean surface variables under different climate scenarios-future change of waves, sea level and wind. Ocean Eng 71:122–129. https://doi.org/10.1016/j.oceaneng.2013.02.016

Morris KR, Sabia S (2016) Pali (was 1C – Central Pacific). In: National Aeronautics and Space Administration (NASA). https://www.nasa.gov/missions/goes/pali-was-1c-central-pacific/?utm_source=chatgpt.com#hds-sidebar-nav-5. Accessed 8 Apr 2025

Muis S, Aerts JCJH, Á. Antolínez JA, Dullaart JC, Duong TM, Erikson L, Haarsma RJ, Apecechea MI, Mengel M, Le Bars D, O'Neill A, Ranasinghe R, Roberts MJ, Verlaan M, Ward PJ, Yan K (2023) Global projections of storm surges using high-resolution CMIP6 climate models. Earths Future 11:e2023EF003479. https://doi.org/10.1029/2023EF003479

Muis S, Verlaan M, Winsemius HC, Aerts JCJH, Ward PJ (2016) A global reanalysis of storm surges and extreme sea levels. Nat Commun. https://doi.org/10.1038/ncomms11969

Neumann B, Vafeidis AT, Zimmermann J, Nicholls RJ (2015) Future coastal population growth and exposure to sea-level rise and coastal flooding: a global assessment. PLoS ONE 10(3):e0118571. https://doi.org/10.1371/journal.pone.0118571

Odériz I, Losada IJ, Silva R, Mori N (2024) Global assessment of interannual variability in coastal urban areas and ecosystems. Environ Res Lett. https://doi.org/10.1088/1748-9326/ad7b5b

Odériz I, Silva R, Mortlock TR, Mori N, Shimura T, Webb A, Padilla-Hernández R, Villers S (2021) Natural variability and warming signals in global ocean wave climates. Geophys Res Lett. https://doi.org/10.1029/2021GL093622

Ordóñez-Zúñiga SA, Correa-Ramírez M, Ricaurte-Villota C, Bastidas-Salamanca M (2021) The Panama Low-Level Jet: extension, annual cycle and modes of variation. Lat Am J Aquat Res 49:750–762. https://doi.org/10.3856/vol49-issue5-fulltext-2591

Portilla J, Caicedo AL, Padilla-Hernández R, Cavaleri L (2015) Spectral wave conditions in the Colombian Pacific Ocean. Ocean Model (Oxf) 92:149–168. https://doi.org/10.1016/j.ocemod.2015.06.005

Portilla-Yandún J (2018) The global signature of ocean wave spectra. Geophys Res Lett 45:267–276. https://doi.org/10.1002/2017GL076431

Portilla-Yandún J, Bidlot J-R (2025) A global ocean spectral wave climate based on ERA-5 data: GLOSWAC-5. J Geophys Res Oceans. https://doi.org/10.1029/2025JC022629

Portilla-Yandún J, Cavaleri L, Van Vledder GP (2015) Wave spectra partitioning and long term statistical distribution. Ocean Model 96:148–160. https://doi.org/10.1016/j.ocemod.2015.06.008

Portilla-Yandún J, Salazar A, Cavaleri L (2016) Climate patterns derived from ocean wave spectra. Geophys Res Lett 43(22):11,736-11,743. https://doi.org/10.1002/2016GL071419

Portilla-Yandún, J., Salazar, A., Sosa, J et al (2020) Modeling multiple wave systems in the eastern equatorial Pacific. Ocean Dynamics 70, 977–990. https://doi.org/10.1007/s10236-020-01370-8

Reguero BG, Losada IJ, Díaz-Simal P, Méndez FJ, Beck MW (2015) Effects of climate change on exposure to coastal flooding in Latin America and the Caribbean. PLoS ONE. https://doi.org/10.1371/journal.pone.0133409

Reguero BG, Losada IJ, Méndez FJ (2019) A recent increase in global wave power as a consequence of oceanic warming. Nat Commun. https://doi.org/10.1038/s41467-018-08066-0

Reguero BG, Méndez FJ, Losada IJ (2013) Variability of multivariate wave climate in Latin America and the Caribbean. Global and Planetary Change 100:70–84. https://doi.org/10.1016/j.gloplacha.2012.09.005

Romero-Centeno R, Zavala-Hidalgo J, Raga GB (2007) Midsummer gap winds and low-level circulation over the eastern tropical Pacific. J Clim 20:3768–3784. https://doi.org/10.1175/JCLI4220.1

Rueda Bayona JG, Rodríguez Rubio E, Ortiz Galvis JR (2007) Caracterización espacio temporal del campo de vientos superficiales del Pacífico colombiano y el Golfo de Panamá a partir de sensores remotos y datos in situ. Boletín Científico CCCP 14:49–68. https://doi.org/10.26640/01213423.14.49_68

Semedo A, Weisse R, Behrens A, Sterl A, Bengtsson L, Günther H (2013) Projection of global wave climate change toward the end of the twenty-first century. Journal of Climate 26:8269–8288. https://doi.org/10.1175/JCLI-D-12-00658.1

Sierra JP, Arias PA, Durán-Quesada AM, Tapias KA, Vieira SC, Martínez JA (2021) The choco low-level jet: past, present and future. Clim Dyn 56:2667–2692. https://doi.org/10.1007/s00382-020-05611-w

Sierra JP, Arias PA, Vieira SC, Agudelo J (2018) How well do CMIP5 models simulate the low-level jet in western Colombia? Clim Dyn 51:2247–2265. https://doi.org/10.1007/s00382-017-4010-5

Silva R, Martínez ML, Hesp PA, Catalan P, Osorio AF, Martell R, Fossati M, Da Silva GM, Mariño-Tapia I, Pereira P, Cienguegos R, Klein A, Govaere G (2014) Present and future challenges of coastal erosion in Latin America. J Coast Res. https://doi.org/10.2112/SI71-001.1

Speranski N, Calliari L (2001) Bathymetric Lenses and Localized Coastal Erosion in Southern Brazil. J Coast Res 209–215

Steenkamp SC, Kilroy G, Smith RK (2019) Tropical cyclogenesis at and near the Equator. Q J R Meteorol Soc 145(722):1846–1864. https://doi.org/10.1002/qj.3529

Torres RR, Giraldo E, Muñoz C, Caicedo A, Hernández-Carrasco I, Orfila A (2022) Seasonal and ENSO-related ocean variability in the Panama Bight. EGUsphere [preprint]

Vallarino Castillo R, Negro Valdecantos V, del Campo JM (2023) Understanding the impact of hydrodynamics on coastal erosion in Latin America: a systematic review. Front Environ Sci. https://doi.org/10.3389/fenvs.2023.1267402

Vallarino-Castillo R, Negro-Valdecantos V, del Campo JM (2024) A systematic review of oceanic-atmospheric variations and coastal erosion in Continental Latin America: historical trends, future projections, and management challenges. J Mar Sci Eng. https://doi.org/10.3390/jmse12071077

Vallarino Castillo R, Negro Valdecantos V, Moreno Blasco L (2022) Shoreline change analysis using historical multispectral Landsat images of the Pacific coast of Panama. J Mar Sci Eng. https://doi.org/10.3390/jmse10121801

Vitousek S, Barnard PL, Fletcher CH, Frazer N, Erikson L, Storlazzi CD (2017) Doubling of coastal flooding frequency within decades due to sea-level rise. Sci Rep. https://doi.org/10.1038/s41598-017-01362-7

Vousdoukas MI, Ranasinghe R, Mentaschi L, Plomaritis TA, Athanasiou P, Luijendijk A, Feyen L (2020) Sandy coastlines under threat of erosion. Nat Clim Chang 10:260–263. https://doi.org/10.1038/s41558-020-0697-0

Yepes J, Poveda G, Mejía JF, Moreno L, Rueda C (2019) Choco-jex: a research experiment focused on the Chocó low-level jet over the far eastern Pacific and western Colombia. Bull Am Meteorol Soc 100:779–796. https://doi.org/10.1175/BAMS-D-18-0045.1

Zhang X, Wu K, Li R, Li D, Zhang S, Zhang R, Li S, Dong X (2023) Analysis of the Interannual variability of Pacific Swell Pools. J Mar Sci Eng. https://doi.org/10.3390/jmse11101883

Zheng C, Li X, Azorin-Molina C, Li C, Wang Q, Xiao Z, Yang S, Chen X, Zhan C (2022a) Global trends in oceanic wind speed, wind-sea, swell, and mixed wave heights. Appl Energy. https://doi.org/10.1016/j.apenergy.2022.119327

Zheng C, Wu D, Wu H, Guo J, Shen C, Tian C, Tian X, Xiao Z, Zhou W, Li C (2022b) Propagation and attenuation of swell energy in the Pacific Ocean. Renew Energy 188:750–764. https://doi.org/10.1016/j.renene.2022.02.071